

Mechanisms for Lagged Atmospheric Response to ENSO SST Forcing

Hui Su, J. David Neelin and Joyce E. Meyerson

September 27, 2004

Department of Atmospheric Sciences
and Institute of Geophysics and Planetary Physics
University of California, Los Angeles

Submitted to the *Journal of Climate*

Corresponding author address:

J. David Neelin

Department of Atmospheric Sciences

University of California, Los Angeles, Los Angeles, CA 90095-1565

e-mail: neelin@atmos.ucla.edu

Abstract

The mechanism and sensitivity of the lagged response of tropical tropospheric temperature to El Niño/Southern Oscillation (ENSO) SST forcing are examined using the quasi-equilibrium tropical circulation model (QTCM) coupled to a slab mixed-layer ocean model, along with a simple analytical model. It is found that the lag and amplitude of tropospheric temperature response depend on mixed-layer ocean depth (MLD), ENSO SST forcing period, areal fraction of mixed-layer ocean and the strength of tropics to midlatitude transports. The phase lag is not a monotonic function of mixed-layer depth. It maximizes at moderate MLD and thus is not very sensitive to MLD in the realistic range. The phase lag asymptotes to values determined by free atmospheric time scales, between 1-2 months, for small or large values of MLD. The amplitude of tropospheric temperature response decreases with increasing MLD. The phase lag and amplitude of tropospheric temperature both increase as specified ENSO SST forcing period increases and they appear rather insensitive to the seasonal cycle of SST. On the other hand, the phase lag and amplitude of mixed-layer ocean SST change monotonically with MLD and ENSO forcing period, with a deeper mixed-layer producing longer lag and smaller amplitude of SST anomalies. Longer ENSO SST forcing periods correspond to longer lag and larger amplitude of mixed-layer ocean SST anomalies. While ENSO region convective heating (precipitation) anomalies are closely tied to SST anomalies, the tropical mean precipitation seems best viewed as a complex by-product of the response rather than as a driver. One useful parameter determining the lag of tropospheric temperature to ENSO SST is the free decay time scale of the coupled system. This parameter combines the effects of surface flux exchanges, heat loss at the top-of-atmosphere and from the tropics to midlatitudes, and finite ocean heat capacity. It is indicative of the extent to which the lagged response of tropical tropospheric temperature to ENSO SST is a coupled phenomenon. Overall, the contribution of coupling to SST outside the ENSO region substantially increases the amplitude and lag of the tropospheric temperature response to ENSO.

1 Introduction

On interannual time scales, variations of tropical mean tropospheric temperature ($\langle \hat{T}' \rangle$) and related variables, such as geopotential height, tend to follow the changes of sea surface temperature (SST) in the equatorial eastern Pacific, with a lag of 1-2 seasons in maximum response (Newell and Weare 1976; Angell 1981; Pan and Oort 1983; Reid et al. 1989; Yulaeva and Wallace 1994; Kumar and Hoerling 2003, hereafter KH03). Because tropospheric temperature variability is important to the inter-basin precipitation teleconnection associated with El Niño/Southern Oscillation (ENSO) (Chiang and Sobel 2002), this lagged relationship can have a complex effect on the precipitation response. For example, there may exist different precipitation anomalies before and after an equilibrium is reached between SST and tropospheric temperature.

Although the lagged thermal response of tropospheric temperature relative to ENSO SST has been noted in many studies using different observations and numerical model simulations, the mechanism for the lagged atmospheric response has yet to be understood. It is known that the tropical troposphere responds rapidly to an anomalous diabatic heating source, via convectively driven Kelvin waves (Heckley and Gill 1984; Jin and Hoskins 1995; Bantzer and Wallace 1996). The time scale associated with this is on the order of a week to 15 days. There must be other slower processes occurring to produce a lag of 1-2 seasons.

On the other hand, a lagged relationship is also known for SST in other basins with respect to Pacific ENSO SST indices (Klein et al. 1999; Enfield and Mayer 1997; Tourre and White 1995; Latif and Barnett 1995). Previous research has suggested that this could occur via the “atmospheric bridge” (Alexander et al. 2002; Lau and Nath 1996; Klein et al. 1999), i.e., through the atmospheric circulation teleconnected to the ENSO SST forcing.

Hence, it is natural to think of the lagged relationship of tropospheric temperature and inter-basin SSTs with regard to ENSO from an integrated coupled perspective. This has been suggested by KH03. They pointed out the role of Indian and Atlantic ocean SSTs for the warming of tropical tropospheric temperature, especially for the lingering of tropospheric warming following the ENSO SST peak. They found a link between the tropical mean rainfall and tropospheric temperature anomalies, but failed to explain the inconsistency of the evolution of rainfall and tropospheric temperature anomalies. Su and Neelin (2003, hereafter SN03) pointed out that on interannual time scales the tropical mean precipitation ($\langle P' \rangle$) is a by-product of the atmosphere-ocean coupled system reaction to the ENSO SST

forcing and it is not a forcing to the system. The connection between boundary SST forcing and tropospheric thermal response has to be considered in a coupled context.

The hypothesis pursued here is as follows. Warmer than normal SST within the Pacific induces a warmer and moister boundary layer and enhances convection. Wave dynamics spreads the warming over the tropics and creates widespread tropospheric temperature warming (Su et al. 2003, hereafter SNM03). The interaction with the ocean surface layer of finite heat capacity could slow part of the tropospheric warming. Then the modified surface flux and top-of-atmospheric radiation due to cloud changes could in turn affect the ocean SST. The purpose of this study is to decompose the coupled atmosphere-ocean response to ENSO SST forcing, focus on the lagged relationship of tropospheric temperature and inter-basin SST, as well as the role of individual processes in determining the amplitude and phase of tropospheric temperature and ocean SST responses.

The tool we use is an intermediate climate model, known as the Quasi-equilibrium Tropical Circulation Model (QTCM), coupled to a slab mixed-layer ocean. The ENSO SST anomalies are prescribed and regarded as an external forcing to the system, similar to Alexander et al. (2002) and KH03. First, numerical experiments are examined to show the nature of the lagged response and sensitivity of lags to different model parameters. Secondly, a simple analytical framework is used to explore the fundamental time scales of the coupled system. Sobel and Gildor (2003) used a similar analytical model of the atmosphere plus a mixed-layer ocean model. They examined the stability of the system to time-dependent oscillations and found steady solutions of the model can become unstable to oscillations on intraseasonal to subannual time scales. We focus on the coupled solutions on interannual time scales. Analytical results are sought for the amplitude and phase of the response of the coupled system to prescribed ENSO SST forcing. The roles of individual physical processes are then analyzed and the mechanism for the lagged response is discussed.

This paper is organized as follows. Section 2 briefly describes the intermediate atmospheric model, the slab mixed-layer ocean model and experimental design. In sections 3 and 4, the observed and modeled lags of tropospheric temperature relative to the Niño-3.4 SST index are shown. Then the sensitivity of the lag to mixed-layer ocean depth, period of SST forcing and SST seasonal cycle is examined in section 5. Following the numerical results, section 6 presents the analytical model of the atmosphere-ocean coupled system and gives the amplitude and lag of tropospheric temperature as a function of mixed-layer depth and period of SST forcing. The decay time scale of the coupled atmosphere-ocean solutions is

given and used to indicate the lag in the forced response. In section 7, the importance of tropical-midlatitude transports for the lag of tropospheric temperature is shown. Summary and discussions are given in section 8.

2 The QTCM and a slab mixed-layer ocean model

We use an intermediate complexity atmospheric circulation model, the QTCM, whose response to ENSO SST forcing has been validated in a number of previous studies (Zeng et al. 2000; Su et al. 2001; Su and Neelin 2002, hereafter SN02; SNM03). The QTCM is a primitive equation model that makes use of the properties of a quasi-equilibrium moist convective closure to simplify vertical structures of atmospheric profile (Neelin and Zeng 2000; Zeng et al. 2000). It includes nonlinear advection, Betts-Miller moist convective adjustment, cloud-radiative interaction, and a simple interactive land model.

The slab mixed-layer ocean model used for this study assumes a fixed mixed layer depth (MLD). A range of values from 0.5 m to 200 m for MLD are tested. The divergence of ocean transport is parameterized using the “Q-flux” correction scheme (Hansen et al., 1988, 1997) where time-averaged surface heat fluxes balance the ocean transport. The Q-flux is obtained from a control run with specified climatological SST. Climatological Q-flux is diagnosed from the seasonal surface fluxes and the time rate of change of SST in the control run, and is used for all runs with a mixed-layer ocean. In this study, we focus on the atmospheric circulation changes associated with ENSO SST forcing. Changes in ocean transport outside the ENSO region are not considered, though these may occur (Latif and Barnett 1995). The mixed-layer ocean interacts with the atmosphere via daily-averaged SST and surface fluxes.

A control run (ObsSST) is driven by observed SST (Reynolds and Smith 1994) from 1950 to 2000. Ten simulations with slightly different initial conditions are conducted and ensemble means are constructed. Since the variability among the 10 members of the ensemble is relatively small compared to ENSO-forced signals, some ensemble means consist of 5 members only. For runs ObsPac+ML, the QTCM is coupled with the mixed-layer ocean except over the main ENSO anomalous SST region, where observed ENSO SST anomalies are used. On the contrary, run ObsPac uses climatological SST outside the ENSO SST region without an interactive ocean. The configuration of the specified ENSO SST region is based on the composite SST difference during December-February between 7 El Niño events and 6 La Niña events over the period of 1950 to 2000. Its outline is approximately

along the 1.0 C contour in the warm minus cold SST composite. The warm events include 1957/58, 1965/66, 1972/73, 1982/83, 1986/87, 1991/92, and 1997/98. The cold events include 1970/71, 1973/74, 1975/76, 1984/85, 1988/89, and 1998/99 (Alexander et al. 2002).

To test the sensitivity of the tropospheric temperature response to ENSO SST forcing, different mixed-layer depths have been used, ranging from 0.5 m to 200 m. Besides using observed SST anomaly as specified forcing, an idealized sinusoidal SST anomaly is used in the SinPac+ML runs. In these runs, different period of SST forcing and various mixed-layer depth are used to provide a detailed picture of the sensitivity of the lag and amplitude of tropospheric temperature response. We have also conducted an experiment in which the phase of maximum SST anomaly is shifted from January to July to examine the role of seasonal cycle. The sensitivity to areal fraction of mixed-layer ocean is tested by replacing part of mixed-layer ocean with climatological SST. Additional experiments are conducted in which anomalies of a particular physical process are suppressed to examine the role of such a process in affecting the lag and amplitude. For example, run ADVCLIM suppresses advection of temperature and moisture anomalies to estimate how important the energy and moisture transports between the tropics and mid-latitude affect the tropospheric temperature response to ENSO SST forcing.

Our analysis focuses on the lead/lag regression of several variables to an ENSO SST index. We use Niño-3.4 SST index (averaged for the area 5N-5S, 170W-120W) as the standard reference for ENSO signal. The lag of a variable with respect to Niño3.4 SST is defined by the month when maximum regression occurs. This may be slightly different from that inferred by comparing two time series, by initiation of response or by other measures of phase relations. For observed tropospheric temperature, we use the National Center for Environmental Prediction (NCEP)/National Center for Atmospheric Research (NCAR) reanalysis data (Kalnay et al. 1996). Tropospheric average refers to the mean between 850 hpa and 200 hpa. Tropical average refers to the mean between 25S and 25N.

3 The observed and modeled tropospheric temperature lag

Previous studies show that ENSO has a strong “phase locking” with seasonal cycle (Rasmusson and Carpenter 1982), although considerable scatter exists for the ENSO onset and termination phases relative to the seasonal cycle (Neelin et al. 2000). The peak warming of

an El Niño usually occurs in the winter time, around December and January. However, the maximum tropical tropospheric temperature warming does not occur until 1-2 seasons later. Figure 1 shows a lead/lag regression of zonally averaged tropospheric temperature anomalies onto the Niño3.4 SST index for the NCEP/NCAR reanalysis and a counterpart in the QTCM control run, ObsSST. The vertical axis labels from -12 to 12, meaning tropospheric temperature leading Niño 3.4 SST 12 months to lagging Niño-3.4 SST 12 months.

For the NCEP/NCAR reanalysis (Fig. 1a), at lag -12 to -6 months (i.e., atmosphere leading Niño-3.4 SST 12-6 months), the tropospheric temperature appears to be negatively correlated with Niño-3.4 SST, likely due to the influence of the previous phase of the ENSO signal. Positive regression of tropical tropospheric temperature anomalies onto the Niño-3.4 SST occurs at all other lags, with a maximum at 3-4 months lag. The lead/lag regression of the modeled temperature onto Niño-3.4 SST (Fig. 1b) is similar to the observations. The maximum regression also occurs at 3 month lag. However, the positive correlation of tropospheric temperature with Niño-3.4 SST begins in May of the year preceding the ENSO peak phase, sooner than the observed, possibly related to the weaker cold temperature anomalies simulated in the model. The regression coefficients are generally smaller for the run ObsSST than for the NCEP/NCAR reanalysis, and they are more confined in the equatorial region.

Figure 2 provides another view of the lagged response of tropospheric temperature to ENSO SST forcing. A time-latitude section of the composite zonally-averaged tropospheric temperature anomalies for a 25-month period is shown, from January of the year preceding an El Niño warm event (month -12) to January of the year after the peak El Niño warming (month 12). The composite is based on four recent El Niño events since 1982, i.e., the 1982/83, 1986/87, 1991/92 and 1997/98 El Niños. A group of 25-calendar-month means, centered on January, are constructed using the four warm events. The January of the peak El Niño warm phase is labeled as month 0. Figure 2a shows the composite for the NCEP/NCAR reanalysis, and Fig. 2c shows the modeled composite for the ObsSST run. The composite Niño-3.4 SST anomaly time series for the 25 months is displayed in Fig. 2b. It can be seen that the warm phase of the composite Niño-3.4 SST anomaly starts in March (month -10) of year -1 and maximizes in January of year 0. It reverses to cold anomalies from October (month 9) of year 0 and is approximately symmetric before and after the peak phase. However, the observed zonally-averaged tropospheric temperature warm anomalies do not occur until May (month -8) of year -1. The peak warming appears around March

(Month 2) of year 0. The modeled tropospheric temperature response captures the lag in maximum warming with slightly weaker amplitude.

The horizontal distribution of simulated tropospheric temperature anomalies is also similar to the NCEP/NCAR reanalysis. Figure 3 shows the composite tropospheric temperature anomalies at 2 month lag, i.e., in March of year 0, for the NCEP/NCAR reanalysis (Fig. 3a) and the QTCM run ObsSST (Fig. 3b). Both modeled and observed composites exhibit a widespread warming across the tropics. The spatial pattern is suggestive of equatorial wave structure: an equatorially symmetric Rossby wave pattern in the eastern Pacific and a Kelvin wave-like structure extending to the east. The modeled temperature response is somewhat weaker than the observed.

4 Lagged response in the coupled atmosphere-mixed-layer-ocean model

A set of experiments, referred to as ObsPac+ML, are conducted to examine the tropospheric temperature lag in the coupled context of atmosphere and mixed-layer ocean. The observed ENSO SST forcing is prescribed within the composite SST anomaly region, and mixed-layer ocean is used elsewhere.

The simulated mixed-layer ocean SST lags the Niño-3.4 by a season or two. Figure 4 shows the regression of global SST anomalies onto the Niño-3.4 SST index at a 5-month lag for observations and the QTCM run ObsPac+ML with a mixed-layer depth of 25 m. The dark outline indicates the region of specified observed SST. Within the Pacific, there is general agreement between the model and the observed. Note that the regression inside the ObsPac box is identical for the observation and the model by design. Cold SST anomalies in the North and South Pacific are simulated, although their locations are restricted to mid-latitudes and maxima occur westward of the observed. The cold SST anomalies in the tropical western Pacific are not simulated, possibly due to lack of ocean dynamics there. The Indian Ocean and tropical north Atlantic Ocean SSTs both positively correlate to ENSO SST at this lag, with modeled amplitude about half of the observed. It has been suggested that ocean dynamics and/or local air-sea interaction may be important for the Indian Ocean SST variability (Webster et al. 1999; Yu and Rienecker 2000; Yu et al. 2002). Thus the atmospheric model coupled with a mixed-layer ocean may not be able to fully capture the SST response.

Figure 5 shows the simulated tropospheric temperature anomaly composite in March of El Niño years from the same ObsPac+ML run. The temperature pattern resembles that in Fig. 3, with a larger positive anomaly area in the western Pacific than in Fig. 3, due to the missing cold SST anomalies there. Nonetheless, the widespread tropospheric temperature warming is reproduced with reasonable strength.

For the ObsPac+ML run with a mixed-layer depth of 25 m, the maximum regression of tropical averaged tropospheric temperature anomalies onto the Niño 3.4 SST index occurs at a 2-month lag, 1 month shorter than the ObsSST run. For comparison, we conduct the ObsPac run, where climatological SST replaces the mixed-layer ocean SST in areas outside the specified ENSO SST. Without an interactive ocean, the lag of tropical tropospheric temperature is reduced to 1 month. Figure 6 shows the resulting lead/lag regression of tropical averaged tropospheric temperature (25S-25N) with respect to Niño 3.4 SST for the ObsSST, ObsPac+ML(25m) and ObsPac runs as well as that for the NCEP/NCAR reanalysis. Clearly, without an active mixed-layer ocean, the lag of tropospheric temperature is relatively short and the amplitude of temperature anomalies is also small compared to model runs with a mixed-layer ocean or observed SST. The results are consistent with KH03 (their Fig. 10). They found that the lag in atmospheric geopotential field exists even without a mixed-layer ocean used and concluded that the lag is not a coupled phenomenon (although their run with a mixed-layer ocean produced a longer lag than their climatological SST run). The ObsSST run has the closest lag to the NCEP/NCAR reanalysis data among three model experiments, although its amplitude of tropospheric temperature anomalies is about 20% lower than the observed. The ObsPac+ML run with 25 m mixed-layer depth produces a similar magnitude of regression of $\langle \hat{T}' \rangle$ to Niño 3.4-SST, but its lag is 2 months shorter than the observed. We note in Fig. 6 that the regression coefficients are not symmetric about the peak, a phenomenon elaborated in KH03. Reasons for this are not clear at this time.

In these experiments, the coupled atmosphere-ocean system responds to specified inter-annual SST forcing in a delayed fashion. The finite heat capacity of the mixed-layer ocean clearly plays a role, but sensitivity to mixed-layer depth and other model parameters is of interest.

5 Sensitivity of the lagged response

For the sensitivity experiments, we use two types of interannual SST forcing. First, the observed SST time series within the composite ENSO region (as shown in Fig. 4) are used in the ObsPac+ML runs. The mixed-layer depth is varied from 0.5 m to 200 m. Another set of experiments, referred to as SinPac+ML, use an idealized sinusoidal SST forcing with varying periods at 2, 3, and 4 years. This aims to identify how the periods of SST forcing impact the lag and amplitude of the tropospheric temperature and SST response.

5.1 Sensitivity to mixed-layer depth

Figure 7 shows the lead/lag regression of tropical averaged tropospheric temperature onto the Niño-3.4 SST index for the ObsPac+ML runs with a MLD of 0.5 m, 25 m, 50 m, 75 m, 100 m, and 200 m. The regression is based on model results from 1982-2000, different from the analysis period used for Fig. 6, which is from 1950 to 2000 with monthly outputs. It is shown that the lags of tropospheric temperature at a MLD of 25 m, 50 m, 75 m and 100 m are all 2.5 months, compared to a lag of 1.5 months for a MLD of 0.5 m and a lag of 2 months for a MLD of 200 m. Differences in lags less than 2 weeks cannot be detected based on biweekly model outputs. The smaller lag for the run with a MLD of 0.5 m is expected due to the smaller heat capacity of the ocean. The amplitude of tropospheric temperature response is higher for smaller MLD. On the other hand, the shorter lag at a MLD of 200 m than those for shallower MLDs seems counter-intuitive. However, we note that the thermal response is smaller when MLD is 200 m than other runs, thus the impact of the ocean onto the troposphere would be smaller than the other runs as well. Considering an extreme case in which the ocean heat capacity is infinitely large, this mixed-layer ocean is equivalent to a fixed-SST lower boundary. Thus the coupled system would tend to have a response time scale solely determined by the atmosphere. It would be shorter than that of the coupled system with moderate MLD. Observed MLD of the tropical ocean ranges from 10 m-100 m (Watterson 2002). The 200 m hypothetical MLD thus suggests an extreme case behavior for the response of the coupled atmosphere-ocean system to interannual SST forcing. Although the lags for tropospheric temperature are not a monotonic function of the mixed-layer depth, the amplitude of the temperature response appears to increase monotonically as MLD decreases. Sobel and Gildor (2003) found that the response of their simple atmosphere/mixed-layer ocean model to intraseasonal disturbance has a non-monotonic dependence on mixed-layer depth. The

maximum response occurs around mixed-layer depth of 10-20 m.

The measure of lag used above refers to the phase delay of the peak response of the tropical tropospheric temperature anomalies with respect to Niño-3.4 SST. The variations of so-defined lag for MLD between 0.5 m and 200 m are within a month, even though the lead/lag regression curves in Fig. 7 appear significantly different for MLD at 0.5 m and MLD at 200 m. Choosing other definitions for lag may result in different numerical values of lags. For example, using the timing of half-amplitude $\langle \hat{T}' \rangle$ response to define lag, the difference between MLD at 0.5 m and 25 m would be about 1.5 months. Considering the asymmetry of the lead/lag regression curve may also provide another measure of lag. For simplicity, we will continue to use the lag of the peak response as our standard measure.

For the mixed-layer ocean SST, the lag relative to Niño-3.4 is longer than the counterpart for tropospheric temperature. Figure 8 shows the lead/lag regression of the model simulated mixed-layer SST outside the ENSO region. The observed tropical mean SST outside the ENSO region and over the whole tropics are also plotted. The observed tropical mean SST has a relatively small lag to Niño-3.4 SST because of the dominance of Niño SST in the average; however, the observed SST outside the ENSO region shows a large lag of about 5 months. The modeled mixed-layer ocean SSTs lag the Niño-3.4 SST 2-10 months, with increasing lag for increasing MLD. The amplitude of SST response, on the other hand, decreases as MLD increases. For a MLD of 25 m, the lag is 4 months; while for a MLD of 50 m, the lag is 5 months, comparable to the observed. The amplitude of SST anomalies is larger than observed in the ObsPac+ML (25 m) or (50 m) runs, possibly due to the lack of simulated cold SST anomalies in the western Pacific (see Fig. 4).

Because convection is an important player in communicating boundary layer forcing to tropospheric temperature warming, it is worth noting how precipitation varies in the coupled system response. Figure 9 shows lead/lag regression of the tropical averaged precipitation for the ENSO region, outside the ENSO region and for the whole tropics. Both the precipitation anomalies inside and outside the ENSO region more or less follow the Niño3.4-SST variations, with little lag behavior. The large cancellation of the positive precipitation anomalies within the ENSO region and negative anomalies outside gives a rather small tropical mean precipitation anomaly. The lag in tropical mean precipitation anomaly tends to be between the lag of tropospheric temperature and that of mixed-layer ocean SST. For realistic mixed layer depths the $\langle \hat{T}' \rangle$ and $\langle P' \rangle$ lags are fairly close, so this might be hard to distinguish in observations. Since the tropical mean rainfall has a different lag behavior than tropospheric

temperature, it argues against viewing it as a driving force for the tropospheric temperature lag. Overall, the precipitation responses inside and outside the ENSO region separately may be more meaningful than the tropical average. The complex relation of tropical mean precipitation lag to other parameters will be examined further in the analytical model.

5.2 Sensitivity to the period of ENSO SST forcing

In runs SinPac+ML, a sinusoidal SST anomaly is specified over the composite ENSO SST region. It is of the form

$$T_s' = T_{s0} \sin(2\pi t/\tau + \phi_o), \quad (5.1)$$

where τ is the period of the SST anomaly forcing, with values of 2, 3 and 4 years. The initial phase ϕ_o is chosen to give a peak warming in January. The spatial form and amplitude of the forcing T_{s0} is based on a composite of ENSO SST anomalies, i.e., $1/2(T_s^{warm} - T_s^{cold})$, where T_s is January SST averaged for warm/cold years.

Figure 10a shows time-evolution of specified SST forcing for a period of 2 years in the run with a MLD of 50 m, and the corresponding time series for tropical averaged tropospheric temperature, mixed-layer ocean SST, and precipitation inside and outside the prescribed SST region. The simulated tropospheric temperature anomalies exhibit a semi-sinusoidal character, with slight departure from a strict sinusoidal curve. It is clear that tropospheric temperature anomalies and mixed-layer ocean SST both lag the specified SST forcing, with the ocean responding in a much slower fashion. The lead/lag regression of the two variables relative to the SST forcing is shown in Fig. 10b. The tropospheric temperature exhibits a lag of two months and the ocean SST has a lag of 4 months. Note that the temperature response before and after the peak SST warming is rather symmetric, different than when observed ENSO SST forcing is used. Since the same SST seasonal cycle is included in the runs ObsPac+ML and SinPac+ML, the seasonal cycle of SST interacting with SST anomalies appears not to be the cause for the asymmetry of tropospheric temperature response shown in Fig. 6 and 7. This contradicts a claim in KH03. The precipitation anomalies appear more closely concurrent with the evolution of SST forcing. The lead/lag regression with the sinusoidal SST forcing shows 0 lag for precipitation inside the SST mask and 1 month lead for the precipitation anomaly outside the SST mask (Fig. 10b). This again confirms that diabatic convective heating is not a driving force to the tropospheric temperature changes, but rather a result of moist convective adjustment to lower boundary forcing.

Figures 11 and 12 summarize the modeled phase lag and amplitude of the tropospheric temperature and mixed-layer ocean SST responses as a function of mixed-layer depth and the period of SST forcing for all SinPac+ML runs. The lags are quantized at 0.5 month by the data interval. Overall, the phase lag of tropospheric temperature is not a monotonic function of MLD. The amplitude of tropospheric temperature, on the other hand, changes rather monotonically with MLD, with a deeper mixed-layer ocean yielding weaker response. Both the phase lag and amplitude increase as the period of SST forcing increases. For mixed-layer ocean SST (Fig. 12), the phase lag increases as the MLD and SST period increase. The amplitude of mixed-layer SST anomaly decreases as MLD increases and it increases when the SST forcing has a longer period. Note that if phase lag scaled by the SST forcing period is plotted as a function of MLD scaled by period (see Appendix), the curves do not overlap. This indicates that time scales other than that given by mixed-layer heat capacity, for example, atmospheric wave dynamics, must come into play.

5.3 Sensitivity to SST seasonal cycle

KH03 mentioned that the lag of tropospheric thermal response with respect to ENSO SST variability and asymmetry of the response about the peak SST warming may be related to seasonal cycle. To test this, we conduct an experiment in which the initial phase, ϕ_o as in (5.1), is chosen to be in July, instead of January. The resulting tropospheric temperature lead/lag regression with the specified forcing is shown in Fig. 10b (indicated by $\langle \hat{T} \rangle'_{ps}$). The phase lag is very similar to the standard run with peak SST warming in January, suggesting that seasonal cycle is not crucial to the lagged response of tropospheric temperature.

5.4 Sensitivity to areal fraction of mixed-layer ocean

It is natural to think that the heat capacity of the mixed-layer ocean is a control factor for the lag of coupled system response. Thus there should exist sensitivity of lags to the area fraction of the mixed-layer ocean in the coupled model. For a smaller area of interactive ocean, a shorter lag is expected. Indeed, experiments in which the Indian Ocean or the Atlantic Ocean mixed-layer SST is replaced by climatological SST confirm that this is the case. Furthermore, the tropospheric thermal response is smaller when the Indian Ocean is non-interactive than when the Atlantic Ocean is non-interactive, although the area of non-interactive ocean is the same for both runs (by construction), suggesting the tropical troposphere may have higher sensitivity to the Indian Ocean SST than to the Atlantic Ocean

SST (SNM03).

6 Exploring the coupled nature of the phase lag analytically

6.1 Derivation

It is obvious that the observed lag of $\langle \hat{T}' \rangle$ with respect to Niño3.4 SST is a result of coupled atmosphere-ocean response to localized SST forcing. Thus, it is tempting to solve the coupled problem in a simple analytical framework to gain insights on the mechanisms for the lagged response.

Following the analytical atmospheric model described in SNM03 and SN03, we add the equation for the mixed-layer ocean component and obtain a coupled atmosphere-ocean system as below:

$$(c_p P_T / g) [\partial_t (\hat{T}' + \hat{q}') + \mathbf{v} \cdot \widehat{\nabla} T' + \mathbf{v} \cdot \widehat{\nabla} q' + (M \nabla \cdot \mathbf{v})'] = R_s' - R_t' + E' + H' \quad (6.2)$$

$$C_M \partial_t T_M' = -R_s' - E' - H', \quad (6.3)$$

where tropospheric temperature and moisture are both in units of K. The $(\hat{\quad})$ represents averages within the troposphere and $(\quad)'$ denotes anomalies. The mixed-layer ocean SST is T_M , while R_s and R_t are radiative fluxes at surface and the top-of-atmosphere (TOA), respectively, with a positive sign for upward fluxes. The surface latent and sensible fluxes are denoted E and H , respectively.

Approximating tropical averaged moisture anomalies as linear with tropospheric temperature anomalies, we use $\langle q' \rangle \approx n \langle T' \rangle$ with $n \approx 0.6$. The $\langle (\quad) \rangle$ denotes tropical averages. The tropical-averaged perturbation surface fluxes and radiative fluxes can be approximately linearized as functions of tropospheric temperature, moisture and SST using empirical flux exchange coefficients as in SNM03 and SN03. The tropical-midlatitude heat and moisture transport terms in (6.2) can also be linearly regressed on temperature anomalies with a parameter ϵ_{tr} . Thus,

$$(c_p P_T / g) \langle \mathbf{v} \cdot \widehat{\nabla} T' + \mathbf{v} \cdot \widehat{\nabla} q' + (M \nabla \cdot \mathbf{v})' \rangle \approx \epsilon_{tr} \langle \hat{T}' \rangle, \quad (6.4)$$

$$R_{s,t}' \approx \epsilon_T^{s,t} \hat{T}' + \epsilon_q^{s,t} \hat{q}' + \epsilon_{T_s}^{s,t} T_s', \quad (6.5)$$

$$\begin{aligned} E' &\approx \rho_a C_H V_s [q'_{sat}(T_s) - q'_{as}] \\ &\approx \epsilon_H \gamma T_s' - \epsilon_H b \hat{T}', \end{aligned} \quad (6.6)$$

$$\begin{aligned}
H' &\approx \rho_a C_H V_s [T_s' - T'_{as}] \\
&\approx \epsilon_H T_s' - \epsilon_H a \hat{T}'.
\end{aligned} \tag{6.7}$$

We use $\epsilon_H = \rho_a C_H V_s$ for the surface flux feedback coefficient. The factors a and b represent ratio of surface air temperature and moisture to tropospheric mean temperature, respectively, with $a \approx 0.7$ and $b \approx 2.0$. The parameter $\gamma = (dq_{\text{sat}}/dT)_{T_s}$ and is about $3 \text{ K } K^{-1}$ for the normal range of SST variations. Note that we ignore the evaporation (and sensible heat flux) changes due to surface wind for simplicity, although this term may not be negligible for many cases of ENSO teleconnection (SN02; Neelin and Su 2004).

In (6.5), (6.6) and (6.7), tropical averages are not given explicitly because we use the same flux exchange coefficients for all tropical regions. The linearization applies locally as well. For compactness, variables in later sections represent tropical averages, except for mixed-layer SST T_M and specified SST forcing T_F , which are averaged over their respective areas. The area fractions of the mixed-layer ocean and the specified SST forcing are σ_M and σ_F , respectively.

6.2 System for spatially averaged \hat{T}' and T_M'

With the above approximations, the rates of change of the tropospheric temperature and mixed-layer ocean SST can be expressed as follows:

$$C_a \partial_t \hat{T}' + [\epsilon_{out}^{net} + (1 - \sigma_L) \epsilon_{sfc}^{net}] \hat{T}' = \epsilon_{T_s}^{net} (\sigma_M T_M' + \sigma_F T_F') \tag{6.8}$$

$$C_M \partial_t T_M' + \epsilon_{T_s}^{net} T_M' = \epsilon_{sfc}^{net} \hat{T}' \tag{6.9}$$

where

$$\epsilon_{out}^{net} = \epsilon_{tr} + \epsilon_{top}^{net}, \quad \epsilon_{top}^{net} = \epsilon_T^t + n \epsilon_q^t \tag{6.10}$$

$$\epsilon_{sfc}^{net} = \epsilon_H b + \epsilon_H a - \epsilon_T^s - n \epsilon_q^s \tag{6.11}$$

$$\epsilon_{T_s}^{net} = \epsilon_{T_s}^s + \epsilon_H \gamma + \epsilon_H \tag{6.12}$$

where ϵ_{out}^{net} is the coefficient for all energy losses out of the tropical troposphere, combining loss coefficients ϵ_{top}^{net} at TOA and ϵ_{tr} to the midlatitudes. Note that tropics-midlatitude moist static energy flux exchange coefficient ϵ_{tr} represents the effect on the total atmospheric column per unit change of tropospheric temperature, similar to radiative fluxes acting on the TOA. The coefficient ϵ_{sfc}^{net} includes the effect of surface radiative fluxes associated with

temperature and moisture changes and the counteracting effect of surface air temperature and moisture change on evaporation and sensible heat fluxes. Another coefficient, $\epsilon_{T_s}^{net}$, is associated with the net surface flux changes per unit change of surface temperature. The small TOA flux loss due to SST, $\epsilon_{T_s}^t$, is omitted.

The values for each flux exchange coefficient are listed in Table 1. Note that ϵ_T^s and ϵ_q^s are negative, corresponding to downward longwave fluxes from the atmosphere to the surface. We ignore cloud-radiative feedback here. Its effect can be considered as a feedback term as in SN02. The equivalent atmospheric heat capacity is $C_a = (c_p P_T/g)(1+n)$.

In the r.h.s. of (6.8), contributions from interactive mixed-layer ocean SST (T_M') and specified ENSO SST forcing (T_F') both appear. On time scales longer than a day, the averaged surface heat fluxes are zero over land regions due to small heat capacity. As a result, no contribution from land fraction σ_L appears in the r.h.s. of (6.8). Similarly, the ϵ_{sfc}^{net} term for the surface flux contributions associated with tropical averaged tropospheric temperature is reduced by the factor $1 - \sigma_L$ due to land fraction.

It is clear from (6.8) and (6.9) that the rate of change of tropospheric temperature and mixed-layer ocean SST in the coupled system evolves differently from an uncoupled system. For tropospheric temperature alone, its free damping time scale is $C_a[\epsilon_{out}^{net} + (1 - \sigma_L)\epsilon_{sfc}^{net}]^{-1}$, determined by the TOA and surface flux exchanges. For mixed-layer ocean SST only, its free damping time scale, $C_M(\epsilon_{T_s}^{net})^{-1}$, is a function of mixed-layer heat capacity and the rate of flux exchange associated with SST variations. The interaction of the troposphere and mixed-layer ocean appears in the r.h.s. of (6.8) and (6.9). The mixed-layer ocean impacts the tropospheric temperature change through surface fluxes; and the tropospheric temperature affects the mixed-layer ocean SST by downward radiative fluxes and surface air temperature and moisture changes, which tend to oppose evaporation and sensible heat flux changes resulting from surface temperature variations. Since the mixed-layer ocean has larger heat capacity than the atmosphere, T_M' evolves at a slower rate, which slows down the tropospheric temperature response to specified ENSO SST forcing.

6.3 Implications for coupled evolution and coupled mode decay

Because the heat capacity of the atmosphere is much smaller than that of the mixed-layer ocean, a useful case is to neglect the term $C_a \partial_t \hat{T}'$ and solve for the eigenvalue of the linear

system. This free decay rate for the coupled system is

$$\lambda = \epsilon_{T_s}^{net} [\epsilon_{out}^{net} + \sigma_F \epsilon_{sfc}^{net}] / [C_M (\epsilon_{out}^{net} + (1 - \sigma_L) \epsilon_{sfc}^{net})]. \quad (6.13)$$

The overall decay time is determined by a combination of the three exchange coefficients, the mixed layer ocean heat capacity and fractions of land and mixed-layer ocean. The term $\sigma_F \epsilon_{sfc}^{net}$ corresponds to the heat loss from the troposphere to the ocean over the specified SST forcing region. For cases with $\sigma_F = 0$, for example, a global warming scenario when forcing is given by radiation, the free decay rate of the coupled system becomes $\lambda = \epsilon_{T_s}^{net} \epsilon_{out}^{net} / [C_M (\epsilon_{out}^{net} + (1 - \sigma_L) \epsilon_{sfc}^{net})]$.

In the QTCM experiments here, land accounts for 26% of the tropics (25S-25N), while the mixed-layer ocean takes up 61% of the tropics. The rest is the specified SST forcing region (13%). Based on the values of flux exchange coefficients in Table 1, the characteristic timescale of the coupled system is $\tau_{coupled} = 1/\lambda = 3.84H$, where H is the MLD in meters and $\tau_{coupled}$ is in days. This yields a decay time scale of 192 days for a MLD of 50 m. If $\sigma_F = 0$, $\tau_{coupled} = 5.24H$, giving a coupled time scale of about 262 days for a MLD of 50 m. For a simpler case, letting $\sigma_L = 0$ and $\sigma_F \rightarrow 0$,

$$\lambda = \epsilon_{T_s}^{net} \epsilon_{out}^{net} / [C_M (\epsilon_{out}^{net} + \epsilon_{sfc}^{net})]. \quad (6.14)$$

The corresponding time scale is $\tau_{coupled} = 6.45H$. For a MLD of 50 m, $\tau_{coupled}$ is 322 days. The coupled time scale is quite sensitive to the area fraction of the mixed-layer ocean since this affects the area with heat capacity relative to the area over which energy loss occurs.

The case (6.14) provides a view of the coupled nature of this mode of decay. If either the surface exchange rates $\epsilon_{T_s}^{net}$ and ϵ_{sfc}^{net} are small, or the TOA-plus-midlatitude loss rate ϵ_{out}^{net} is small, then the *slower* rate determines the overall decay. In other words, both the flux exchange between the mixed-layer ocean and atmosphere, and the loss from the tropical atmosphere are crucial processes. The coupled time scale is longer than one would expect from linearized SST decay alone, which is given by $C_M / \epsilon_{T_s}^{net}$, corresponding to a time scale of 85 days for a MLD of 50 m.

Considering a sinusoidal SST forcing as in (5.1), (6.8) and (6.9) can be solved without neglecting C_a to obtain the phase lag and amplitude of the tropospheric temperature and mixed-layer ocean SST as functions of mixed-layer depth, SST forcing period, areal fractional of the mixed-layer ocean, and various flux exchange coefficients. The full solution is given in the Appendix. Numerical values of the analytical solutions at reasonable mixed-layer depths

and SST forcing periods are shown in Fig. 13 and 14. Again, we find the phase lag of tropospheric temperature is not a monotonic function of MLD and maximizes at moderate MLD. It increases as the period of SST forcing increases. The amplitude of temperature response decreases as MLD increases, and increases as the forcing period increases. For mixed-layer ocean SST, the lag increases monotonically for larger mixed-layer depths. Its amplitude also decreases monotonically with mixed-layer depth. Longer period ENSO SST forcing would be associated with longer lag and stronger amplitude of mixed-layer ocean SST. Discussion of scaling the lag curves in Fig. 13a by the period of SST forcing is given in the Appendix.

The equations (6.8) and (6.9) give insight into why this system behaves differently as a function of period or mixed-layer heat capacity than expected from the usual forced-damped mixed layer ocean. Because the forcing occurs via the atmospheric equation (6.8) and large C_M implies small T_M' , the atmosphere approximately responds to T_F' alone. The lag in $\langle \hat{T}' \rangle$ for large C_M (at a given forcing period) is due to the fast atmospheric adjustment and is thus small.

The role of the atmospheric time scale in the phase lag dependence may be seen by comparing the solid curve for a 3 year period in Figure 13a (which includes C_a) to the long-dash-dotted curve (which does not). The two curves appear shifted by the amount associated with atmospheric internal heat capacity (corresponding to a time scale of 0.5 months). With $C_a = 0$, the phase lag goes to zero at both high (not shown) and low values of C_M . At high C_M , this occurs because $T_M' \rightarrow 0$ and there is no ocean effect on the fast atmosphere; at low C_M neither fluid has significant heat capacity. When $C_a \neq 0$, the atmospheric time scale limits how small the phase lag can get as C_M varies.

Another useful case to consider for (6.8)-(6.9) is a switch-on problem where T_F' is increased suddenly and then held constant. Because atmosphere and mixed-layer ocean time scales are very different, initially T_M' remains small, while \hat{T}' increases rapidly to balance with T_F' . Then as T_M' equilibrates on time scale $\tau_{coupled}$, \hat{T}' can increase further in balance with T_F' plus the current value of T_M' in (6.8). Thus \hat{T}' has two stages of warming, one fast, but limited by energy loss to T_M' , and one slow, on a slaved coupled time scale, limited by energy loss to space and midlatitudes.

Comparing Figs. 13 and 14 to Figs. 11 and 12, the analytical model results of phase lag and amplitude are consistent with those from the numerical simulations, although exact values differ. This may be due to our simplified flux linearization, averaging over atmospheric

wave dynamics, and neglect of cloud-radiative feedback, etc.

6.4 Precipitation

It is possible to solve the tropical averaged precipitation anomalies in the coupled system using (6.8) and a moisture equation as in SN03 (their eq.(3.2)). The resulting tropical mean precipitation is

$$\langle P' \rangle = C_a(1+n)^{-1} \partial_t \hat{T}' + [\epsilon_{out}^{Tnet} + (1 - \sigma_L) \epsilon_{sfc}^{Tnet}] \hat{T}' - \epsilon_{T_s}^{Tnet} (\sigma_M T_{M'} + \sigma_F T_{F'}), \quad (6.15)$$

where the flux exchanges coefficients ϵ_{out}^{Tnet} , ϵ_{sfc}^{Tnet} and $\epsilon_{T_s}^{Tnet}$ are similar to their counterparts in (6.8) except they that do not include the moisture transport between the tropics and midlatitudes and terms associated with evaporation.

$$\epsilon_{out}^{Tnet} = \epsilon_{tr}^T + \epsilon_T^t + n \epsilon_q^t, \quad (6.16)$$

$$\epsilon_{sfc}^{Tnet} = \epsilon_{Ha} - \epsilon_T^s - n \epsilon_q^s \quad (6.17)$$

$$\epsilon_{T_s}^{Tnet} = \epsilon_{T_s}^s + \epsilon_H. \quad (6.18)$$

The coefficient ϵ_{tr}^T is the regression coefficient of tropics-midlatitude dry static energy transport onto $\langle \hat{T}' \rangle$

$$(c_p P_T / g) \langle \mathbf{v} \cdot \widehat{\nabla} T' + (M_s \nabla \cdot \mathbf{v})' \rangle \approx \epsilon_{tr}^T \langle \hat{T}' \rangle, \quad (6.19)$$

where M_s is the ‘‘gross dry stratification’’ (Neelin and Zeng 2000). The value of ϵ_{tr}^T is usually larger than ϵ_{tr} because the averaged dry static energy transport tends to cancel with moisture transport.

Substituting for $\langle \hat{T}' \rangle$ using (6.8) and assuming a sinusoidal SST forcing of frequency ω , we have

$$\langle P' \rangle = \left(\frac{[\frac{C_a}{(1+n)} i\omega + \epsilon_{out}^{Tnet} + (1 - \sigma_L) \epsilon_{sfc}^{Tnet}]}{[C_a i\omega + \epsilon_{out}^{net} + (1 - \sigma_L) \epsilon_{sfc}^{net}] \epsilon_{T_s}^{net} - \epsilon_{T_s}^{Tnet}} \right) (\sigma_M T_{M'} + \sigma_F T_{F'}). \quad (6.20)$$

In the above expression, the tropical mean precipitation anomalies depend on a weighted combination of SST anomalies in forcing and mixed layer regions. The proportionality factor results from canceling effects of various flux coefficients. Depending on the exact values of these coefficients, the real part of this factor can be positive or negative and tends to be small. With the values of flux exchange coefficients as in Table 1, the tropical mean precipitation has a lag relative to specified SST forcing that lies between the lag of tropospheric temperature and the lag of mixed-layer ocean SST. The lag of precipitation anomalies does not control the lag for tropospheric temperature. For example, keeping the same MSE transport rate

(ϵ_{tr}) and varying the moisture transport, changes in (ϵ_{tr}^T) would give different precipitation lag but have no effect in tropospheric temperature lag. This again supports the view that precipitation is merely a by-product of the coupled atmosphere-ocean response.

7 Role of mid-latitude transports

The moist static energy transport from the tropics is not a dominant term in budgets for seasonal tropospheric temperature anomaly (SNM03), but such transport has a non-negligible role in determining the lag of tropospheric temperature relative to SST. The linear regression of tropical-averaged moist static energy transport anomalies onto the tropical-averaged tropospheric temperature anomalies yields a coefficient of $5.4 \text{ Wm}^{-2}\text{K}^{-1}$, comparable to the coefficient for the TOA radiative flux associated with tropospheric temperature changes. The moist static energy transport anomalies act as a damping to the tropospheric temperature change. The equivalent damping time scale is about 10 days. Without moist static energy transport, the analytical results yield much longer phase lag and a larger amplitude of tropospheric temperature response. For example, the phase lag and amplitude of $\langle \hat{T}' \rangle$ increases by 50% when the MSE transport is ignored for a SST forcing period of 3 year, shown in Fig. 13a dashed line. A QTCM experiment (run ADVCLIM) is conducted in which the anomalies of MSE transport are reduced by replacing advection terms $\mathbf{v} \cdot \widehat{\nabla} T'$ and $\mathbf{v} \cdot \widehat{\nabla} q'$ by their climatological values. The resulting lead/lag regression of $\langle \hat{T}' \rangle$ relative to Niño-3.4 SST forcing is shown in Fig. 15. Compared to the corresponding control run with a lag of 2 months, the temperature lag increases to 3 months and the anomaly amplitude is increased by 60%. Thus, the MSE transport between the tropics and mid-latitudes is an important process limiting the thermal response of the troposphere to the ENSO SST forcing.

8 Summary and Discussion

Tropical averaged tropospheric temperature variations lag ENSO SST in the eastern Pacific by a few months. SST in other basins also exhibits a lag relationship with eastern Pacific SST. Although the atmospheric temperature lag exists even when no atmosphere-ocean coupling is allowed (for instance, in run ObsPac), coupling with an ocean mixed-layer slows the tropospheric response to a significant extent. The pattern of tropospheric temperature warming resembles that expected from wave dynamics, but warming outside the ENSO region

increases on a time scale longer than that of the atmospheric wave adjustment process. A number of numerical experiments and a simple analytical model are used to examine the mechanism and sensitivity of the phase lag and amplitude of the tropospheric temperature response to ENSO SST forcing. The QTCM and approximate analytical results are roughly comparable to the observed, using peak response as a measure of lag.

It is found that tropospheric temperature lag is not a monotonic function of mixed-layer ocean depth. It maximizes at moderate mixed-layer depths, about 25-100 m. In the limit of large or small mixed-layer depth, the phase lag asymptotes to values given by free atmospheric time scales. In QTCM results, the lag is 1.5 months for small MLD. With observed ENSO SST forcing, the QTCM-simulated tropospheric temperature phase lag varies with MLD rather insensitively, ranging from 1.5 months for very small MLD to 2.5 months for the 25-100 m of MLD range, and dropping again for larger MLD (Fig. 7). The amplitude of $\langle \hat{T}' \rangle$ decreases as MLD increases. For the mixed-layer ocean SST, increasing MLD yields monotonically longer lag and much smaller amplitude. The small mixed-layer ocean SST response adds little to the atmospheric warming, which is why the tropospheric temperature lag becomes small when MLD is sufficiently large. The phase lag and amplitude of the tropospheric temperature response appear not to be sensitive to SST seasonal cycle. Area fractions of interactive ocean and land impact the response time scale significantly. In a case when anomalies of temperature and moisture advection from the tropics to midlatitudes are suppressed in the model, the phase lag increases substantially. In experiments with sinusoidal SST forcing, the phase lag and amplitude of $\langle \hat{T}' \rangle$ increase significantly with forcing period.

Using a simply analytical model framework, it is clear that the exchange of fluxes at the atmosphere-ocean interface, and the atmospheric energy loss to space and to the midlatitudes greatly impact the time scales at which the atmosphere and ocean respond to external forcing. As a result, the coupled time scale involves the combined effect of radiative fluxes at top-of-atmosphere and at surface, surface heat fluxes, and tropics-midlatitude moist static energy transports, compounded with mixed-layer heat capacity.

The slowing of decay rate of the tropospheric temperature by the ocean is illustrated in a simple experiment which—interpreted using analytical model (6.8) and (6.9) results—summarizes the underlying physics well enough that we use it as a conclusion. In this experiment, we impose a constant positive SST anomaly of 2 degrees inside the composite ENSO SST region for the first 8 months, then turn it off afterwards. The rest of the ocean is a 50 m mixed-layer. The response time series of tropical-averaged tropospheric temperature

and mixed-layer ocean SST are plotted in Fig. 16. A component of $\langle \hat{T}' \rangle$ responds fairly quickly, within in a month or two. This time scale is associated with fast surface flux adjustment and wave dynamics for tropospheric temperature only. As other ocean regions warm due to teleconnected surface flux change and cloud-radiative feedback, the $\langle \hat{T}' \rangle$ and mixed-layer ocean SST have a slower, co-varying signal. The warming of the coupled system peaks near the end of the positive ENSO forcing and stays positive for a substantial period after the SST forcing is turned off. After an initial fast decay of part of the atmospheric signal, there is a roughly exponential joint decay of $\langle \hat{T}' \rangle$ and T'_M with a time scale of about half a year. On the other hand, the precipitation has characteristics different from $\langle \hat{T}' \rangle$ and T'_M . It has a sudden response in the beginning to the SST forcing, then evolves more or less along with the combined mixed-layer ocean and tropospheric temperature changes. Analytic work indicates that it is not a driver for the tropospheric temperature change, but a by-product of the atmosphere and ocean coupled response to interannual SST forcing.

The exponential growth/decay of the mixed-layer SST and tropospheric temperature that appears in both the spin-up and decay phases is consistent with a coupled tropospheric temperature and SST mode found in the analytical model. The characteristic time scale τ_{coupled} of this coupled mode depends on SST-troposphere flux exchange coefficients and coefficients for the TOA and midlatitude energy loss, as noted in (6.13). Both the flux exchange between the mixed-layer ocean and atmosphere, and the loss from the tropical atmosphere to space and to midlatitudes are important processes determining the coupled mode contribution to the lag of tropospheric temperature. This coupled mode contribution, due to interaction with SST outside the ENSO region, substantially increases the amplitude and lag of the tropospheric temperature response to ENSO.

Acknowledgments. This work was supported under National Science Foundation Grant ATM-0082529, National Oceanographic and Atmospheric Administration Grant NA16-GP2003 and National Aeronautics and Space Administration Grant NA-GS-9358. This is UCLA IGPP contribution 6212. The authors thank A. Kumar and M. P. Hoerling for sharing their pre-published manuscript. Discussions with F.-F. Jin and A. H. Sobel are appreciated.

Appendix

A Solutions to the analytical model

The state dynamics of the coupled atmosphere mixed-layer ocean in response to a sinusoidal SST forcing can be described by the following equations:

$$\partial_t T' + m_{11} T' + m_{12} T_M' = \sigma_F \epsilon_{T_s}^{net} T_{s0} \sin(\omega t) \quad (\text{A.21})$$

$$\partial_t T_M' + m_{21} T' + m_{22} T_M' = 0 \quad (\text{A.22})$$

where the amplitude of the SST forcing is T_{s0} and ω is the forcing frequency. For simplicity, we use $f_0 = \sigma_F \epsilon_{T_s}^{net} T_{s0} / C_a$ in derivations below. The coefficients m_{ij} ($i = 1, 2; j = 1, 2$) are combinations of flux exchange coefficients and heat capacity of the atmosphere or the mixed-layer ocean.

$$m_{11} = [\epsilon_{out}^{net} + (1 - \sigma_L) \epsilon_{sfc}^{net}] / C_a \quad (\text{A.23})$$

$$m_{12} = -\sigma_M \epsilon_{T_s}^{net} / C_a \quad (\text{A.24})$$

$$m_{21} = -\epsilon_{sfc}^{net} / C_M \quad (\text{A.25})$$

$$m_{22} = \epsilon_{T_s}^{net} / C_M. \quad (\text{A.26})$$

It is straight forward to solve the set of linear equations (6.8) and (6.9) in response to a sinusoidal SST forcing:

$$\begin{aligned} \hat{T}'(t) &= \hat{T}'(\omega) \sin(\omega t + \phi - \Delta\phi_T) + C_T^+ \exp(-\gamma_+ t) + C_T^- \exp(-\gamma_- t) \\ T_M'(t) &= T_M'(\omega) \sin(\omega t + \phi - \Delta\phi_{T_M}) + C_{T_M}^+ \exp(-\gamma_+ t) + C_{T_M}^- \exp(-\gamma_- t), \end{aligned} \quad (\text{A.27})$$

where γ_{\pm} are the damping rates in the coupled system, which are the eigenvalues of matrix m_{ij} ($i = 1, 2; j = 1, 2$)

$$\gamma_{\pm} = \frac{1}{2} \left[(m_{11} + m_{22}) \pm \sqrt{(m_{11} - m_{22})^2 + 4m_{12}m_{21}} \right]. \quad (\text{A.28})$$

The amplitudes C_T^{\pm} and $C_{T_M}^{\pm}$ can be found according to the initial conditions. The first terms in the equations (A.27) are the inhomogeneous terms which is the long term solution while the rest two terms are the homogeneous solutions which decay away as t becomes much larger than the damping scales. The lag phases and amplitudes for the inhomogeneous terms

are expressed as

$$\hat{T}(\omega)e^{-i\Delta\phi_{\hat{T}}} = \frac{f_0(i\omega + m_{22})}{(i\omega + m_{11})(i\omega + m_{22}) - m_{12}m_{21}} \quad (\text{A.29})$$

$$T_M(\omega)e^{-i\Delta\phi_{T_M}} = -\frac{f_0m_{21}}{(i\omega + m_{11})(i\omega + m_{22}) - m_{12}m_{21}}. \quad (\text{A.30})$$

Now let us study the lag as a function of the frequency of the external forcing ω . Note that the lag time is simply the phase divided by ω , using Eqs. (A.30),

$$\text{lag}_{\hat{T}}(\omega) \equiv \Delta\phi_{\hat{T}} = \frac{1}{\omega} \tan^{-1} \left[\frac{\omega(\omega^2 + m_{22}^2 + m_{12}m_{21})}{m_{11}\omega^2 + m_{22}(m_{11}m_{22} - m_{12}m_{21})} \right], \quad (\text{A.31})$$

$$\text{lag}_{T_M}(\omega) \equiv \Delta\phi_{T_M} = \frac{1}{\omega} \cot^{-1} \left[\frac{m_{11}m_{22} - m_{12}m_{21} - \omega^2}{\omega(m_{11} + m_{22})} \right]. \quad (\text{A.32})$$

When we ignore the rate of change of tropospheric temperature due to small heat capacity of air, the decay rate of the coupled system is

$$\lambda = (m_{11}m_{22} - m_{12}m_{21})/m_{11} \quad (\text{A.33})$$

which yields (6.13). The solutions for $\langle \hat{T}' \rangle$ and T_M are

$$\hat{T}' = \frac{(i\omega + m_{22})}{m_{11}(i\omega + \lambda)} f_0 \quad (\text{A.34})$$

$$T_M' = \frac{-m_{21}}{m_{11}(i\omega + \lambda)} f_0. \quad (\text{A.35})$$

Thus the phase lag of $\langle \hat{T}' \rangle$ is

$$\Delta\phi_{\hat{T}} = \omega^{-1}(\tan^{-1}m_{22}/\omega - \tan^{-1}\lambda/\omega). \quad (\text{A.36})$$

Note that since there is a single time derivative term in this approximation, one can rescale the equation as follows: $\Delta\phi_{\hat{T}}^* = \omega\Delta\phi_{\hat{T}}$, $m_{22}^* = C_M m_{22}$, $\lambda^* = C_M \lambda$, $\omega^* = C_M \omega$ and thus obtain a function independent of C_M .

$$\Delta\phi_{\hat{T}}^* = (\tan^{-1}m_{22}^*/\omega^* - \tan^{-1}\lambda^*/\omega^*). \quad (\text{A.37})$$

Hence, rescaling phase lag and C_M by forcing period in Fig. 13a would yield one curve, if the effects of atmospheric time scale associated with C_a were negligible.

References

- Alexander, M. A., I. Blade, M. Newman, J. R. Lanzante, N-C Lau, and J. D. Scott, 2002: The atmospheric bridge: the influence of ENSO teleconnections on air-sea interaction over the global oceans. *J. Climate*, **15**, 2205-2231.
- Angell, J. K., 1981: Comparison of variations in atmospheric quantities with sea surface temperature variations in the equatorial eastern Pacific. *Mon. Wea. Rev.*, **109**, 230-243.
- Bantzer C. H., and J. M. Wallace, 1996: Intraseasonal variability in tropical mean temperature and precipitation and their relation to the tropical 40-50 day oscillation. *J. Atmos. Sci.*, **53**, 3032-3045.
- Chiang, J., and A. H. Sobel, 2002: Tropical tropospheric temperature variations caused by ENSO and their influence on the remote tropical climate. *J. Climate*, **15**, 2616–2631.
- Enfield, D. B., and D. A. Mayer, 1997: Tropical Atlantic sea surface temperature variability and its relation to El Niño-Southern Oscillation. *J. Geophys. Res.*, **102**, 929–945.
- Hansen, J., I. Fung, A. Lacis, D. Rind, S. Lenedeff, R. Ruedy, and G. Russell, 1988: Global climate changes as forecast by Goddard Institute for Space Studies three-dimensional model. *J. Geophys. Res.*, **93**, 9341-9364.
- Hansen, J., R. Ruedy, A. Lacis, G. Russell, M. Sato, J. Lerner, D. Rind, and P. Stone, 1997: Wonderland climate model, *J. Geophys. Res.*, **102**, 6823-6830.
- Heckley, W. A., and A. E. Gill, 1984: Some simple analytical solutions to the problem of forced equatorial long waves. *Quart. J. Roy. Meteor. Soc.*, **110**, 203-217.
- Jin, J., and B. Hoskins, 1995: The direct reponse to tropical heating in a baroclinic atmosphere. *J. Atmos. Sci.*, **52**, 307-319.
- Latif, M., and T. P. Barnett, 1995: Interactions of the tropical oceans. *J. Climate*, **8**, 952–968.
- Lau, N.-C., and M. J. Nath, 1996: The role of the “atmospheric bridge” in linking tropical Pacific ENSO events to extratropical SST anomalies. *J. Climate*, **9**, 2036–2057.
- Kalnay, E., et al., 1996: The NCEP/NCAR 40-year reanalysis project. *Bull. Amer. Meteor. Soc.*, **77**, 437–471.
- Klein, S. A., B. J. Soden, and N.-C. Lau, 1999: Remote sea surface temperature variations during ENSO: evidence for a tropical atmospheric bridge. *J. Climate*, **12**, 917–932.
- Kumar, A. and M. P. Hoerling, 2003: The nature and causes for the delayed atmospheric response to El Niño. *J. Climate*, **16**, 1391-1403.
- Neelin, J. D., and N. Zeng, 2000: A quasi-equilibrium tropical circulation model—formulation. *J. Atmos. Sci.*, **57**, 1741–1766.

- Neelin, J. D., F-F. Jin, and H-H. Syu, 2000: Variations in ENSO phase locking. *J. Climate*, **13**, 2570-2590.
- Neelin, J. D., and H. Su, 2004: Moist teleconnection mechanisms for the tropical South American and Atlantic sector during El Niño. *J. Climate*, *submitted*.
- Newell, R. E., and B. C. Weare, 1976: Ocean temperatures and large scale atmospheric variations. *Nature*, **262**, 40–41.
- Pan, Y. H., and A. H. Oort, 1983: Global climate variations connected with sea surface temperature anomalies in the eastern equatorial Pacific Ocean for the 1958-73 Period. *Mon. Wea. Rev.*, **111**, 1244–1258.
- Rasmusson, E. M., and T. H. Carpenter, 1982: Variations in tropical sea surface temperature and surface wind fields associated with the Southern Oscillation/ El Niño. *Mon. Wea. Rev.*, **110**, 354–384.
- Reid, G. C., K. S. Gage, and J. R. McAfee, 1989: The thermal response of the tropical atmosphere to variations in equatorial Pacific sea-surface temperature. *J. Geophys. Res.*, **94**, 14705–14716.
- Reynolds, R. W., and T. M. Smith, 1994: Improved global sea surface temperature analyses using optimum interpolation. *J. Climate*, **7**, 929–948.
- Sobel, A. H., and H. Gildor, 2003: A simple time-dependent model of SST hot spots. *J. Climate*, **16**, 3978-3992.
- Su, H., J. D. Neelin, and C. Chou, 2001: Tropical teleconnection and local response to SST anomalies during the 1997-1998 El Niño. *J. Geophys. Res.*, **106**, 20,025–20,043.
- Su, H., and J. D. Neelin, 2002: Teleconnection mechanisms for tropical Pacific descent anomalies during El Niño. *J. Atmos. Sci.*, **59**, 2682-2700.
- Su, H., J. D. Neelin, and J. E. Meyerson, 2003: Sensitivity of tropical tropospheric temperature to sea surface temperature forcing. *J. Climate*, **16**, 1283-1301.
- Su, H., and J. D. Neelin, 2003: The scatter in tropical average precipitation anomalies. *J. Climate*, **16**, 3966-3977.
- Toure, Y. M., and W. B. White, 1995: ENSO signals in global upper-ocean temperature, *J. Phys. Oceanogr.*, **25**, 1317–1332.
- Watterson, I. G., 2002: The sensitivity of subannual and intraseasonal tropical variability to model ocean mixed-layer depth. *J. Geophys. Res.*, **107**, 10.1029/2001JD000671.
- Webster, P. J., A. M. Moore, J. P. Loschnigg, and R. R. Leben, 1999: Coupled ocean-atmosphere dynamics in the Indian Ocean during 1997-98. *Nature*, **401**, 356-360.
- Yu, L., and M. M. Rienecker, 2000: Indian Ocean warming of 1997-1998. *J. Geophys. Res.*,

105, 16923–16939.

Yu, J., C. R. Mechoso, J. C. McWilliams, and A. Arakawa 2002: Impacts of the Indian Ocean on the ENSO cycle, *Geophys. Res. Lett.*, **29(8)**, 1204, doi:10.1029/2001GL014098.

Yulaeva, E. and J. M. Wallace, 1994: The signature of ENSO in global temperature and precipitation fields derived from the microwave sounding unit. *J. Climate*, **7**, 1719-1736.

Zeng, N., J. D. Neelin, and C. Chou, 2000: A quasi-equilibrium tropical circulation model—implementation and simulation. *J. Atmos. Sci.*, **57**, 1767–1796.

Table 1: The values of the flux exchange coefficients for the analytical model (in units of $Wm^{-2}K^{-1}$).

	Corresponding flux	Value
ϵ_T^t	TOA longwave flux change due to \hat{T}'	3.0
ϵ_q^t	TOA longwave flux change due to \hat{q}'	-1.8
$\epsilon_{T_s}^t$	TOA longwave flux change due to T_s'	0.3
ϵ_T^s	Surface longwave flux change due to \hat{T}'	-3.3
ϵ_q^s	Surface longwave flux change due to \hat{q}'	-5.5
$\epsilon_{T_s}^s$	Surface longwave flux change due to T_s'	6.28
ϵ_H	Surface heat fluxes associated with surface drag and winds	5.5
ϵ_{tr}	Tropics-midlatitude MSE transports regressed on \hat{T}'	5.4
ϵ_{top}^{net}	Net TOA longwave flux change due to \hat{T}' and \hat{q}'	1.9
ϵ_{out}^{net}	Net flux loss from the troposphere regressed on \hat{T}'	7.3
ϵ_{sfc}^{net}	Net surface flux exchange due to \hat{T}'	21.5
$\epsilon_{T_s}^{net}$	Net surface flux change due to T_s'	28.3

Figure Captions

Figure 1. Regression of zonally averaged tropospheric temperature onto the Niño-3.4 SST index for (a) the NCEP/NCAR reanalysis and (b) the QTCM run ObsSST. The lead-lag regressions are calculated relative to climatological means for the period of 1950 to 2000. Negative (positive) y-axis values indicate months for which the target variable leads (lags) the Niño-3.4 index. Negative contours are dashed. Regression values above/below ± 0.1 have medium/light shading, with dark shading above 0.2.

Figure 2. Composite evolution of zonally averaged tropospheric temperature anomalies from 12 months before and 12 months after the January of peak El Niño events. (a) for the NCEP/NCAR reanalysis and (c) for the QTCM run ObsSST. (b) Same composite anomalies of Niño-3.4 SST index based on the four El Niño events for the period of 1982-1998. Positive anomalies greater than 0.2 C are shaded.

Figure 3. Composite of zonally averaged tropospheric temperature anomalies in March of the El Niño years (0), close to the peak tropospheric temperature warming. (a) for NCEP/NCAR reanalysis and (b) for the QTCM run ObsSST. Composite is based on the four El Niño events from 1982 to 1998. Positive anomalies greater than 0.2 C are shaded.

Figure 4. Regression of SST onto the Niño-3.4 SST index at 5-month lag for (a) observed SST and (b) simulated SST in the run ObsPac+ML, with a mixed-layer depth of 25 m. Dark/light shading above/below ± 0.1 . Contour interval is 0.1 C.

Figure 5. As in Fig. 3 but for the QTCM run ObsPac+ML (MLD=25 m).

Figure 6. Lead/lag regression coefficients of tropical tropospheric temperature anomalies onto the Niño-3.4 SST index for the NCEP reanalysis, the QTCM run ObsSST, ObsPac+ML(MLD = 25 m), and run ObsPac. Corresponding lags for maximum regression values are marked.

Figure 7. Lead/lag regression coefficients of tropical tropospheric temperature anomalies

onto the Niño-3.4 SST index for the QTCM runs ObsPac+ML at different mixed-layer depths ranging from 200 m to 0.5 m. Corresponding mixed-layer depths are shown above the curves, and lags for maximum regression values are marked.

Figure 8. Lead/lag regression coefficients of averaged mixed-layer ocean SST onto the Niño-3.4 SST index for the QTCM runs ObsPac+ML. The dark solid line is for observed ocean SST outside the specified ENSO SST region and the light gray dashed line refers to SST anomalies averaged over the whole tropics.

Figure 9. Similar to Fig. 7 but for averaged precipitation anomalies outside and inside the specified ENSO SST forcing region (expressed as contributions to the tropical average) as well as tropical average precipitation (25S to 25N).

Figure 10. (a) Time series of model simulated anomalies of area averaged mixed-layer ocean SST (C), tropical mean tropospheric temperature (C), precipitation ($mmday^{-1}$) averaged inside and outside the SST forcing mask regions from a SinPac+ML run with a MLD of 50 m and SST forcing period of 2 years. The specified SST forcing is indicated by the time series of the Niño3.4 SST index. (b) Lead/lag regression coefficients of the variables in (a) onto the Niño3.4 SST index. The curve marked by $\langle \hat{T} \rangle'_{ps}$ refers to the simulated tropospheric temperature lead/lag regression when the peak phase of SST forcing is shifted by 6-months.

Figure 11. (a) Phase lag (months) and (b) amplitude (C) of tropical average tropospheric temperature anomalies as functions of mixed-layer depth and period of idealized SST forcing for all QTCM SinPac+ML runs.

Figure 12. As in Fig. 11 except for model-simulated mixed-layer ocean SST.

Figure 13. Analytical model (a) phase lag (months) and (b) amplitude (C) of tropical average tropospheric temperature anomalies as functions of mixed-layer depth and SST forcing period. The solid curves correspond to full solutions to (6.8) and (6.9). The dashed curves correspond to results when MSE transports to mid-latitudes are ignored. The long-

dash-dotted line corresponds to the lag of tropospheric temperature when atmospheric heat capacity is neglected for a SST forcing period of 3 years.

Figure 14. Analytical model (a) phase lag (months) and (b) amplitude (C) of mixed-layer ocean SST as functions of mixed-layer depth and SST forcing period.

Figure 15. Lead/lag regression coefficients of tropical tropospheric temperature anomalies onto the Niño-3.4 SST index for the QTCM run ObsPac+ML (MLD=50 m) with and without advection anomalies. Corresponding lags for maximum regression values are marked by dashed lines.

Figure 16. Evolution of tropical-averaged tropospheric temperature and mixed-layer ocean SST anomalies outside the ENSO SST forcing region along with the specified SST forcing for a QTCM simulation with an ENSO SST anomaly switched on for 8 months then switched off.

\hat{T} regression on Nino3.4 SST

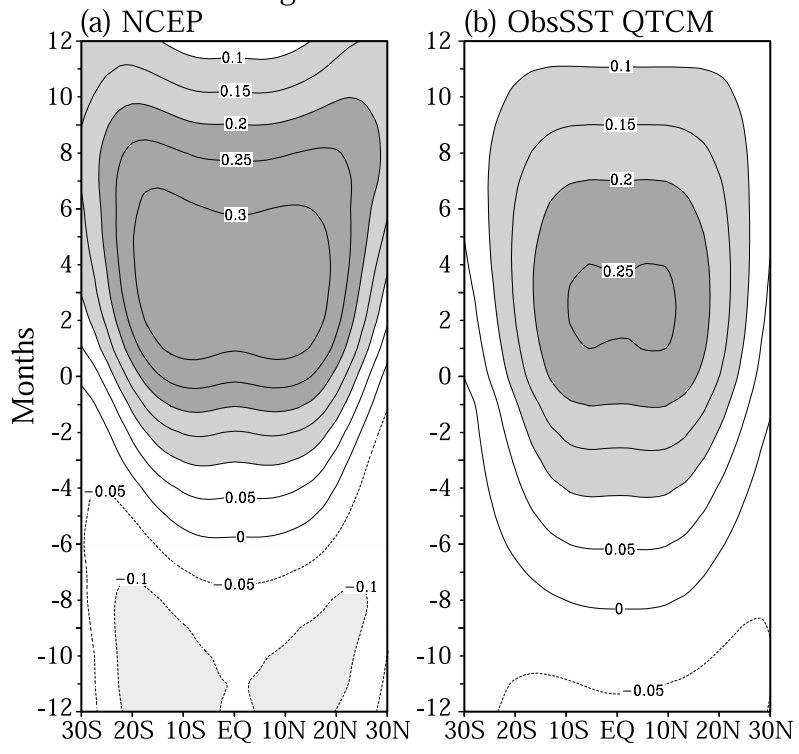


Figure 1

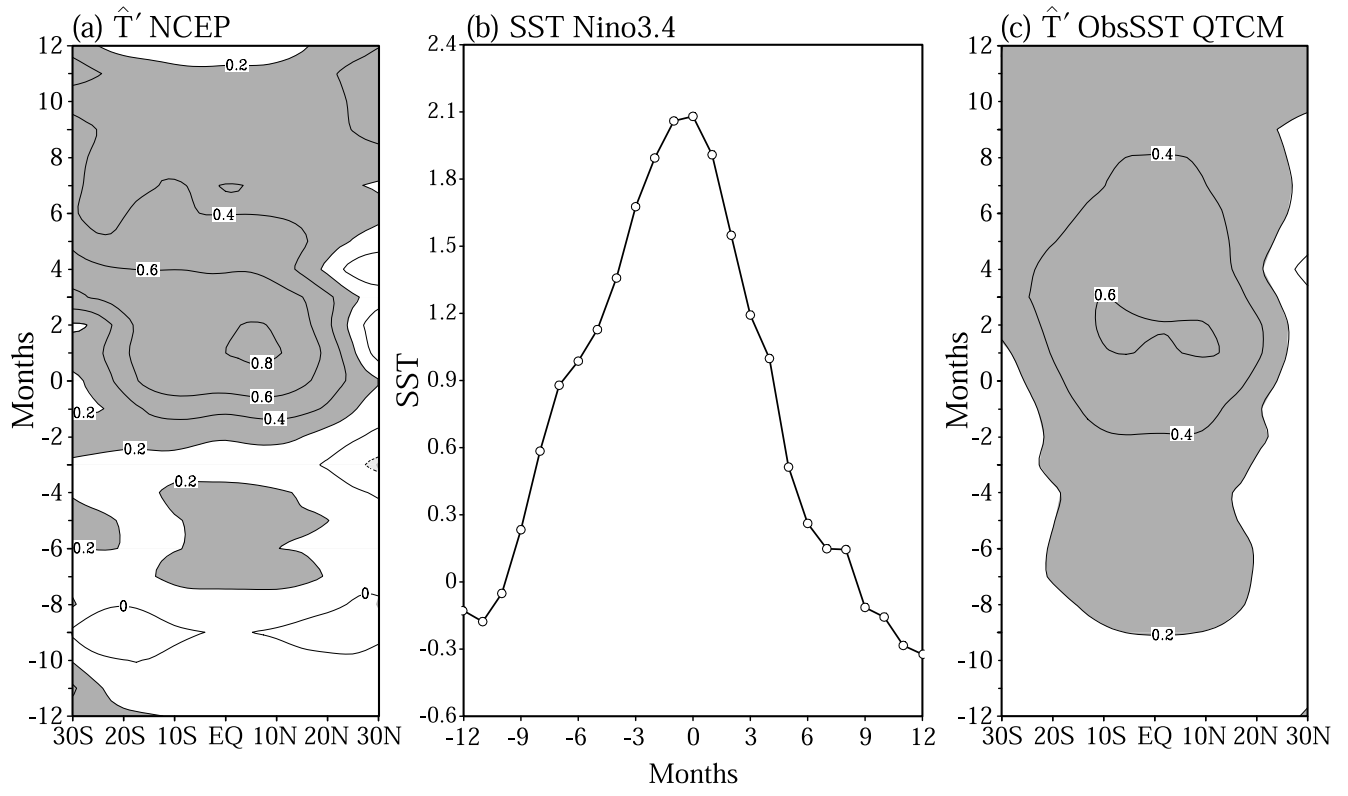
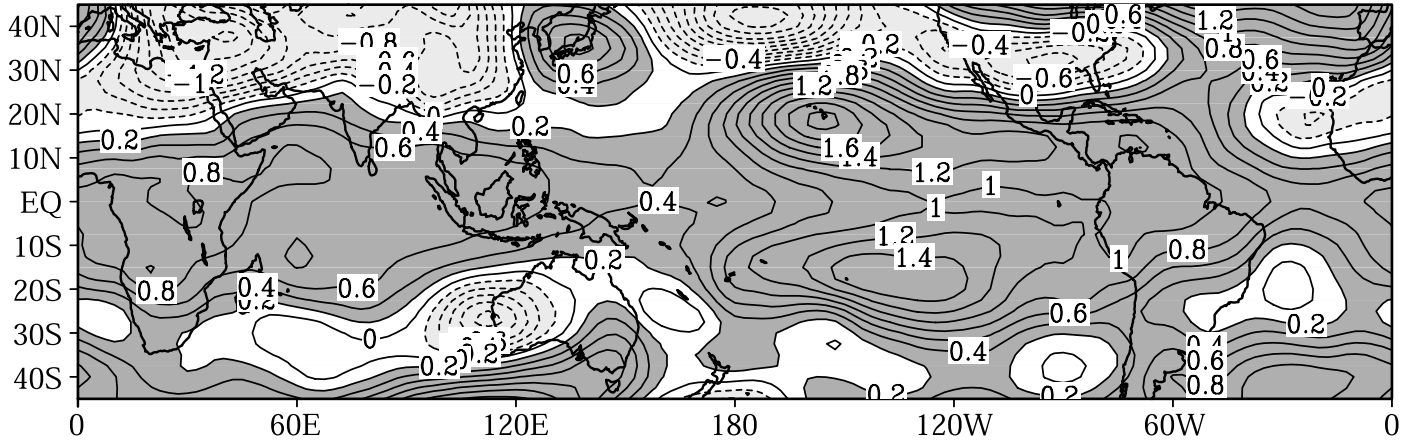


Figure 2

(a) \hat{T}' Composite March Year 0 NCEP



(b) \hat{T}' Composite March Year 0 ObsSST QTCM

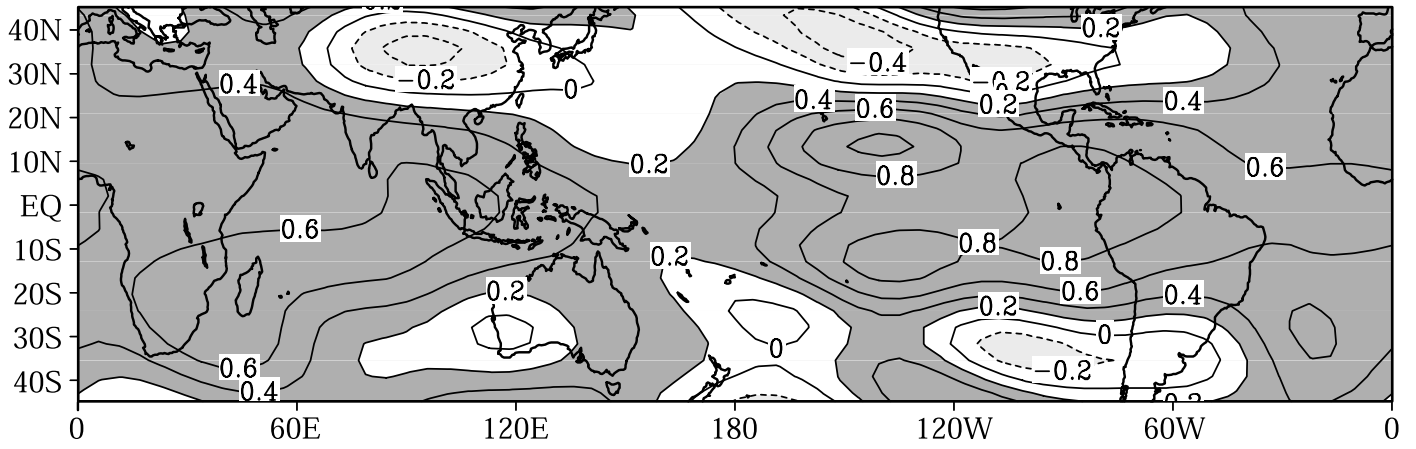
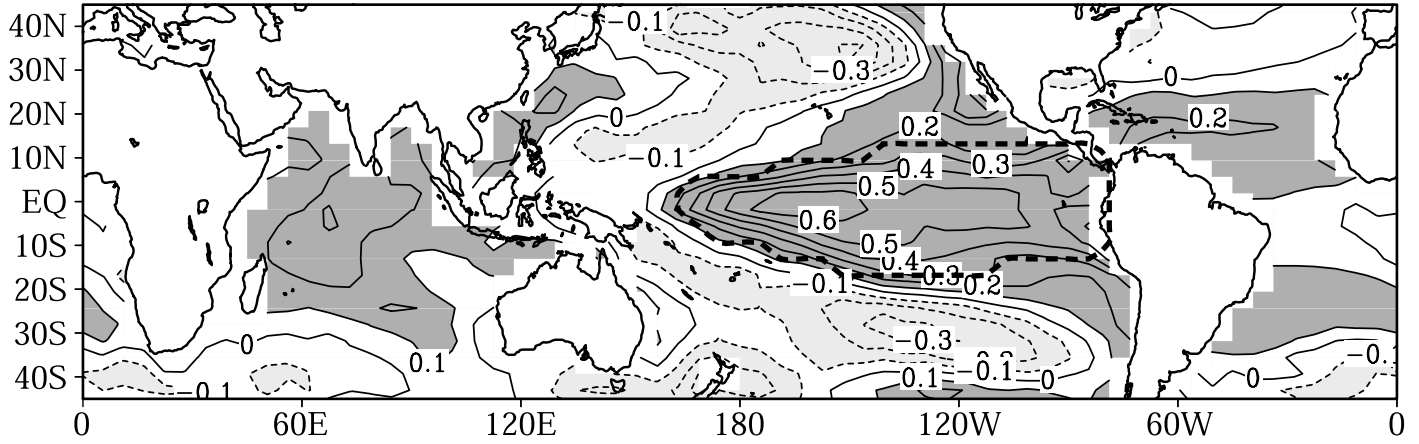


Figure 3

(a) SST 5-month lag regression to Nino3.4 OBS



(b) ObsPac + ML(25m)

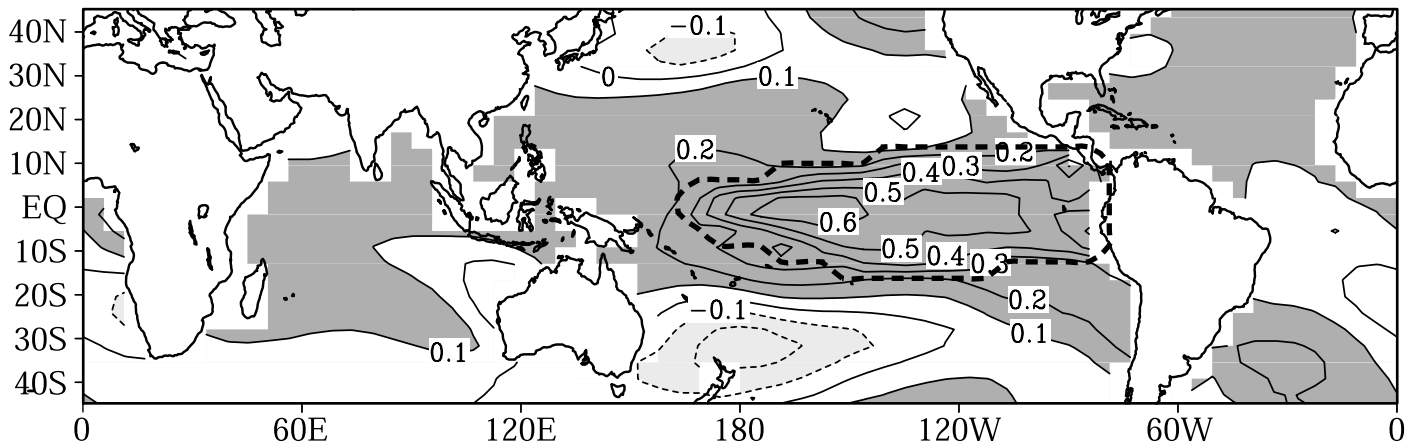


Figure 4

\hat{T}' Composite March Year 0 ObsPac + ML(25m) QTCM

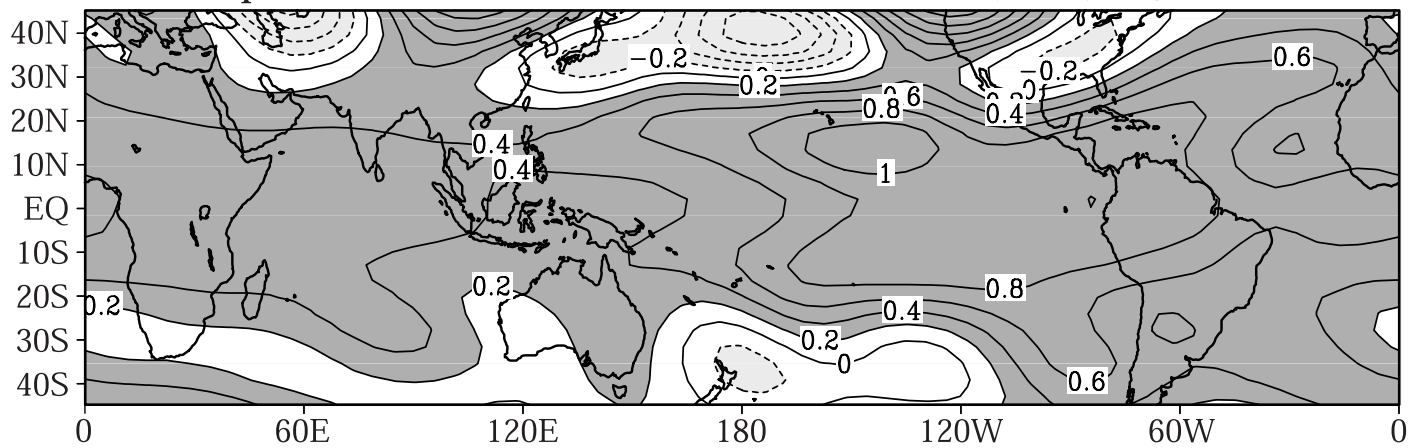


Figure 5

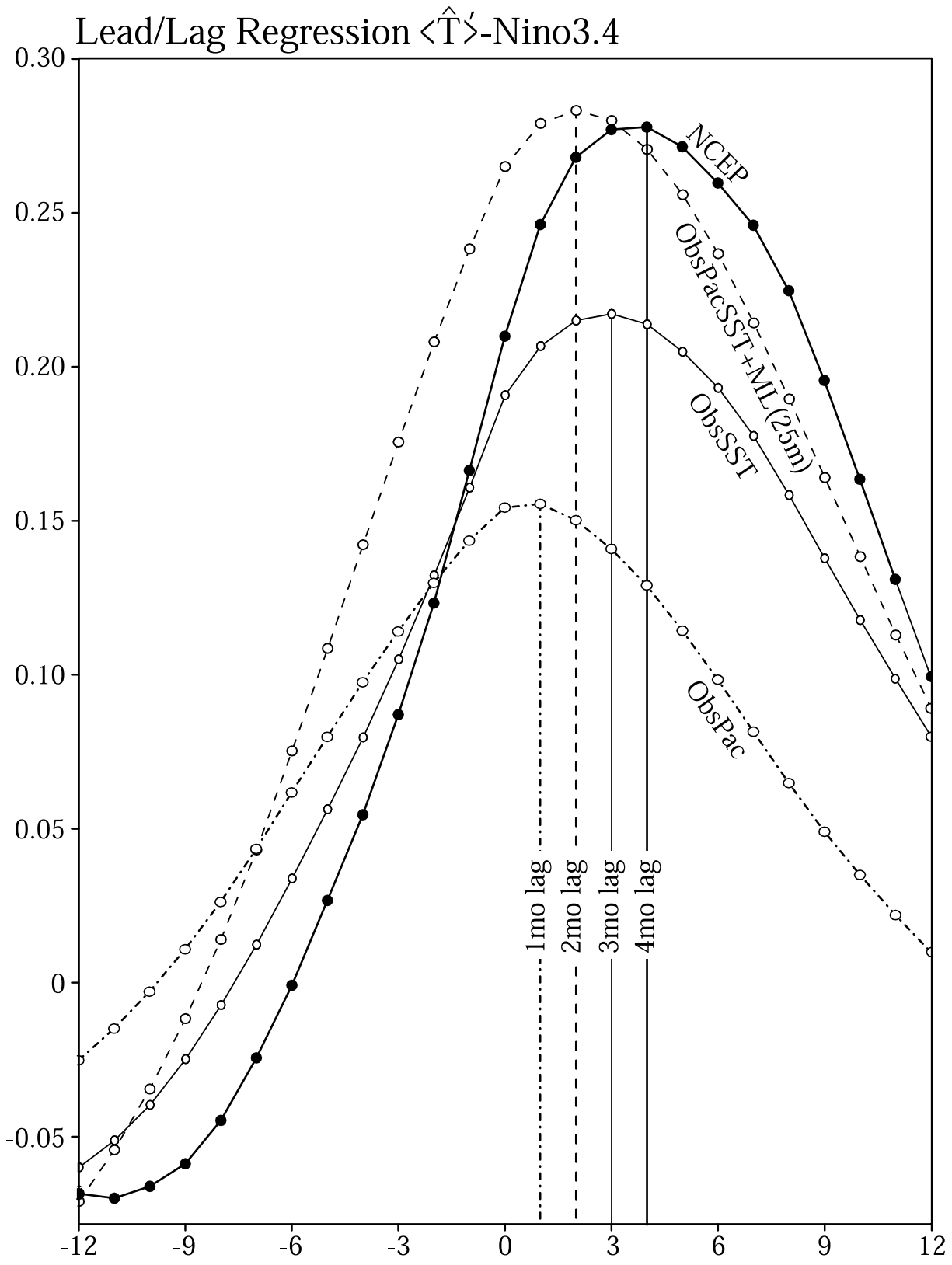


Figure 6

Lead/Lag Regression $\langle \hat{T}' \rangle$ -Nino3.4

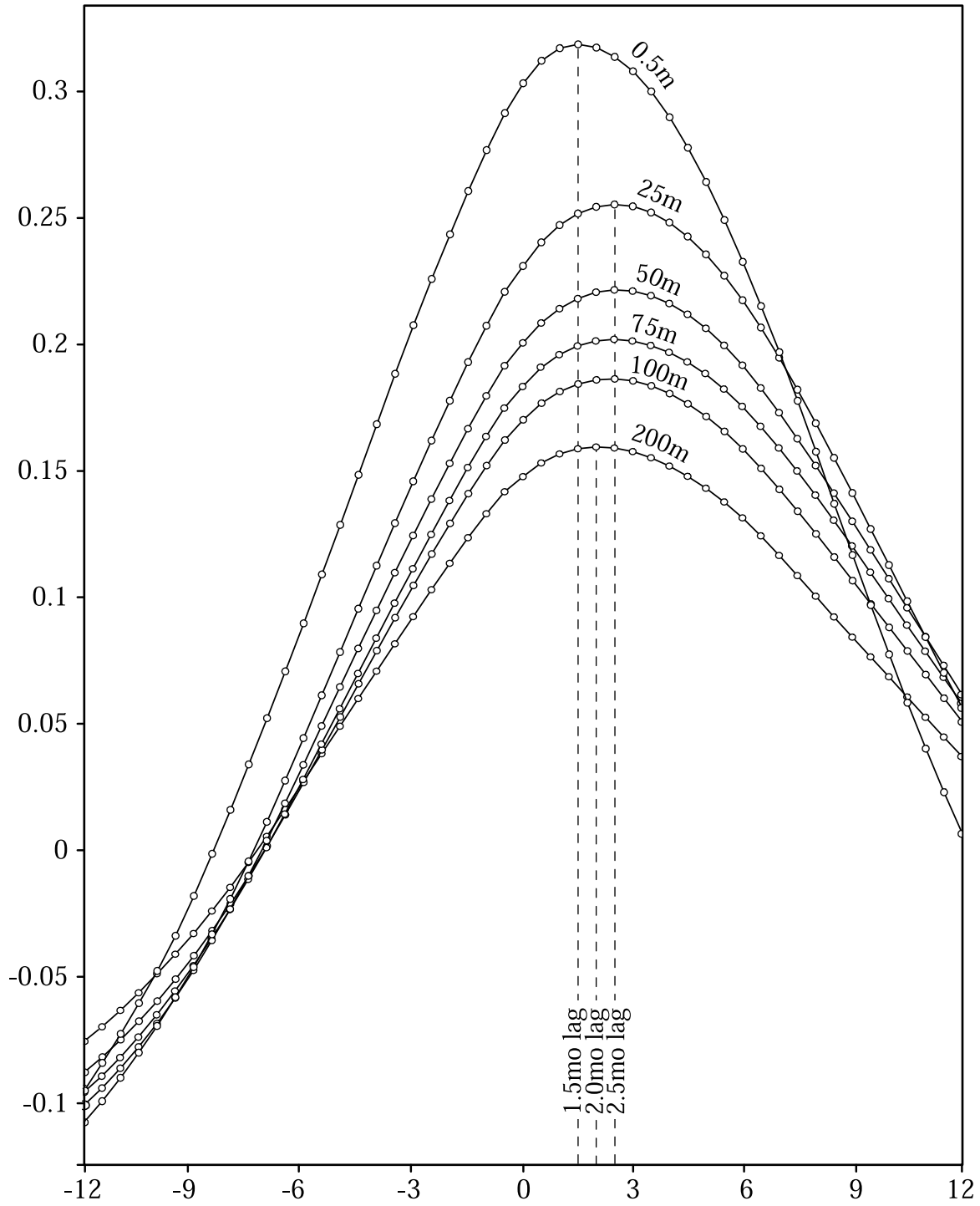


Figure 7

Lead/Lag Regression SSTa-Nino3.4

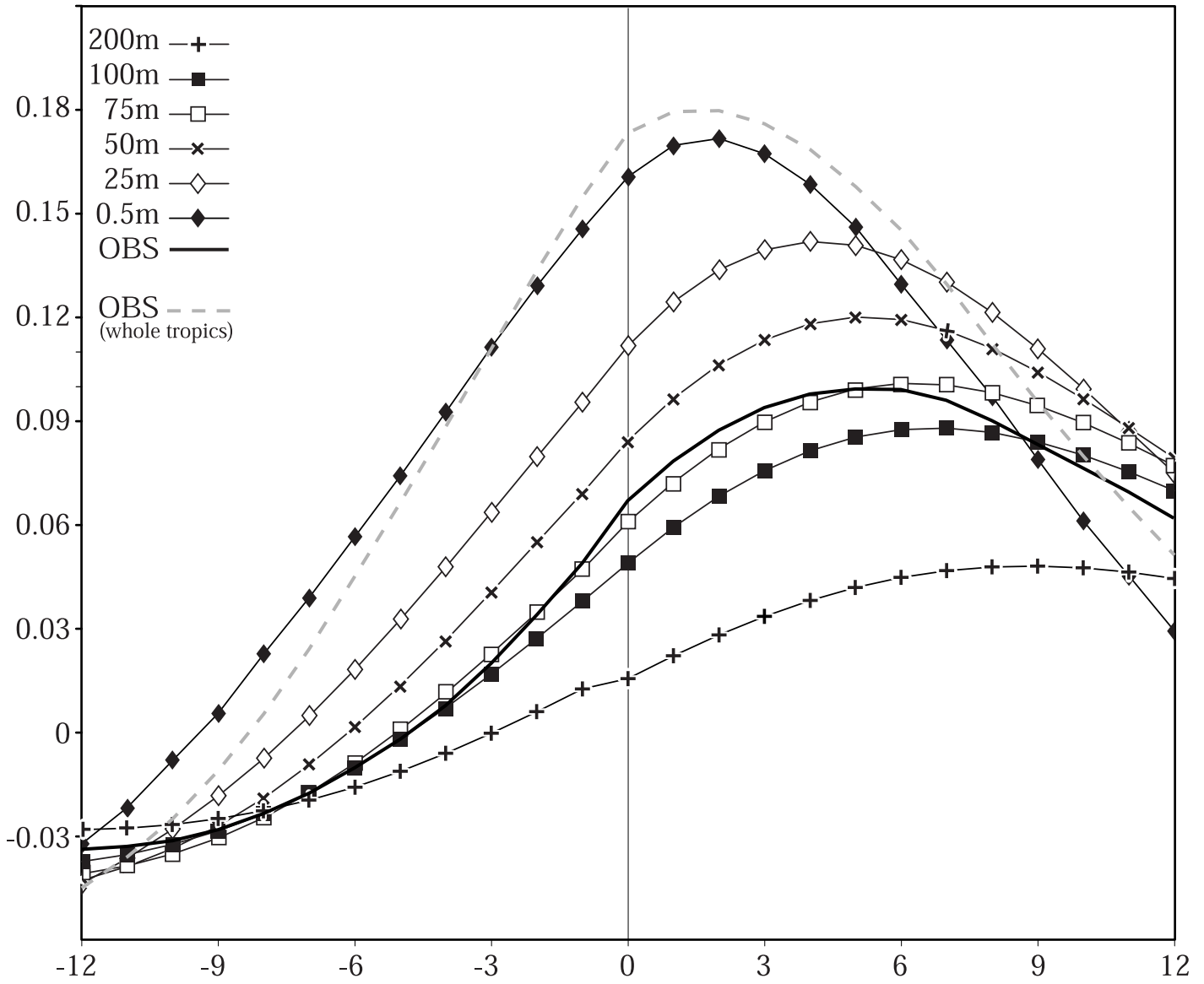


Figure 8

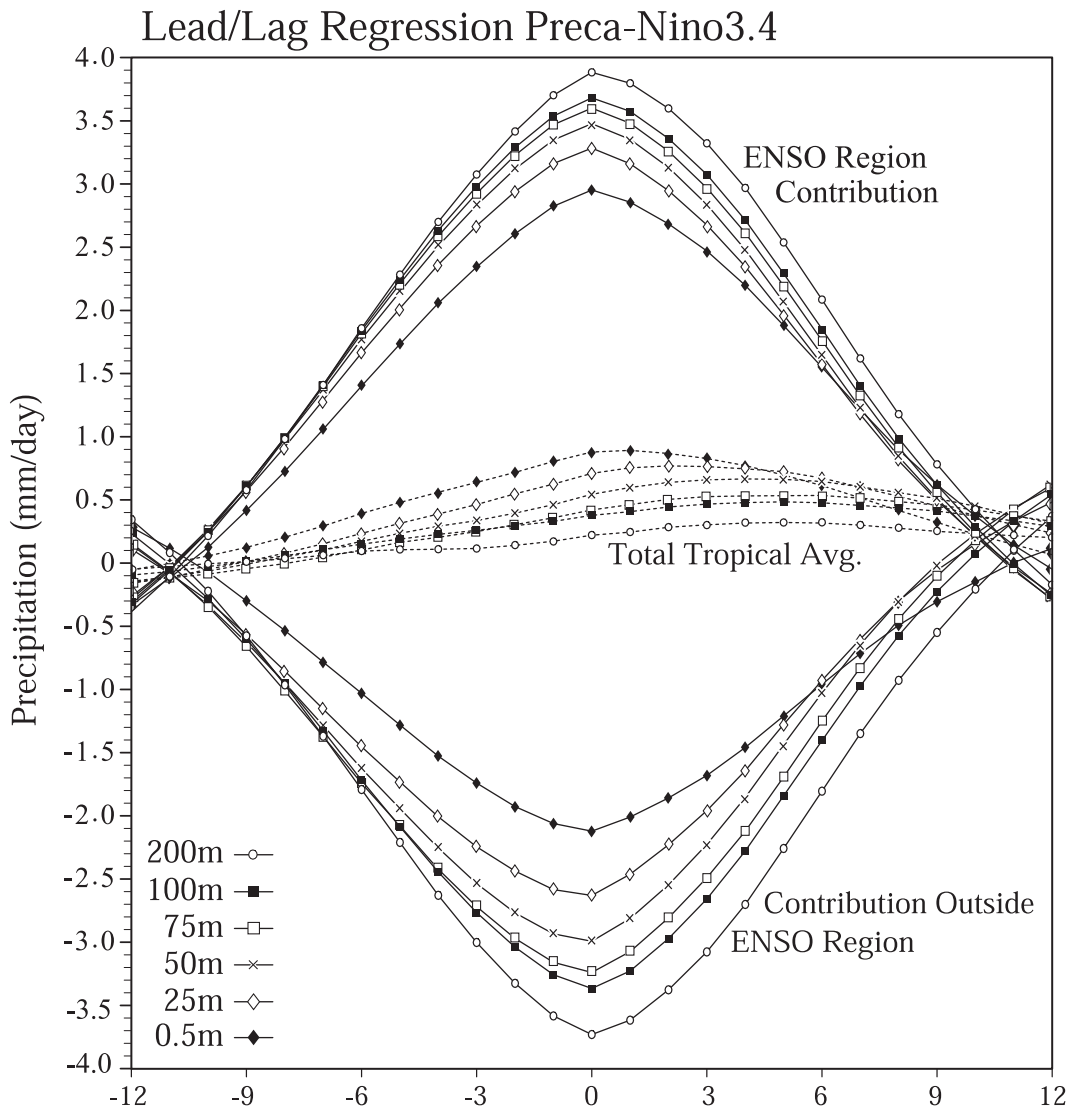
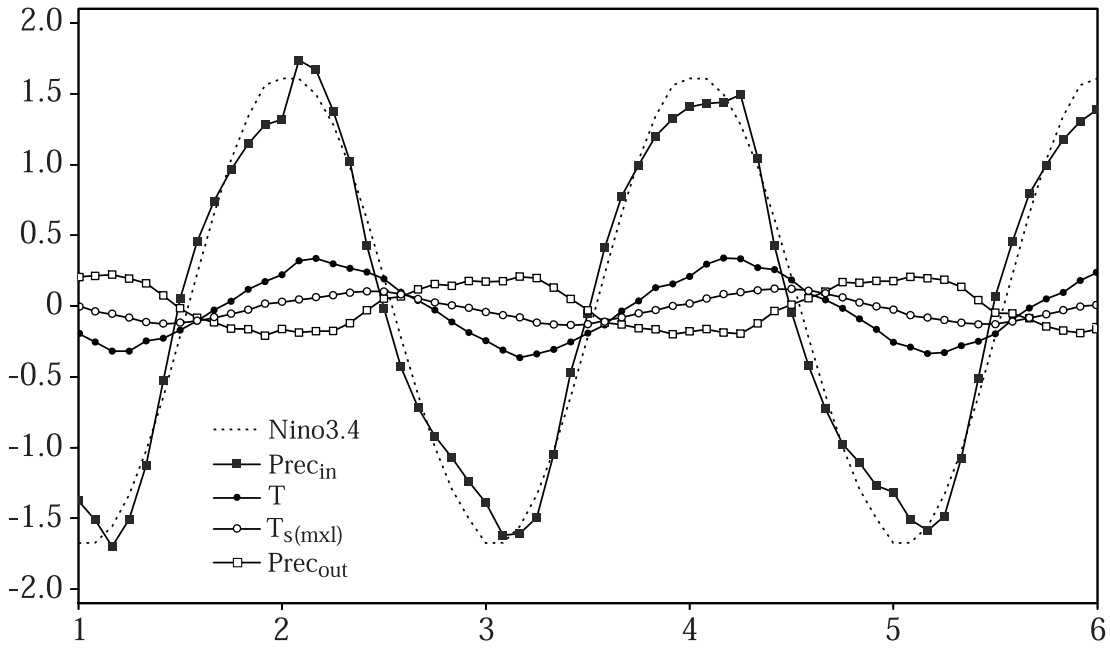


Figure 9

(a) 2 yr. SinPac+ML(50m) Time Evolution



(b) Lead/Lag Regression 50m MixLayer (2yr. SinPac+ML(50m))

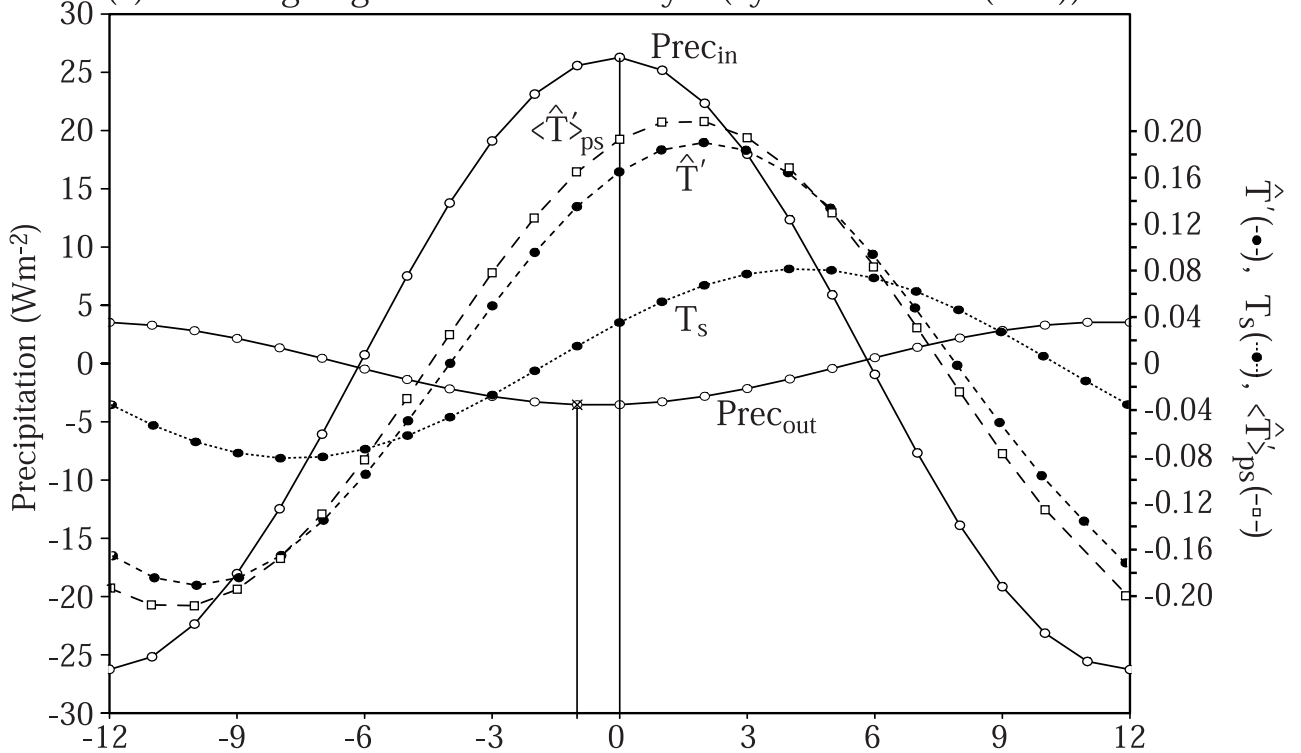


Figure 10

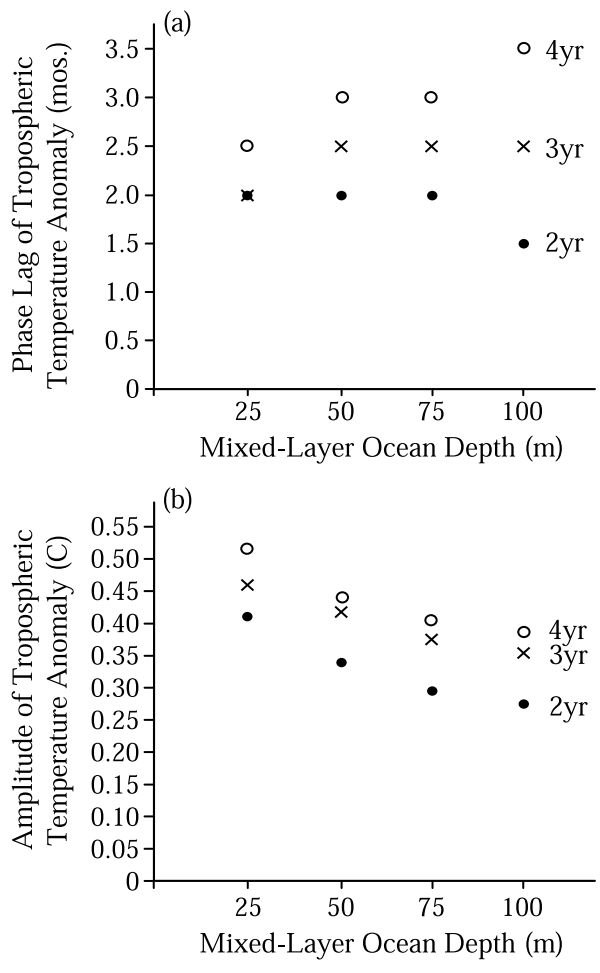


Figure 11

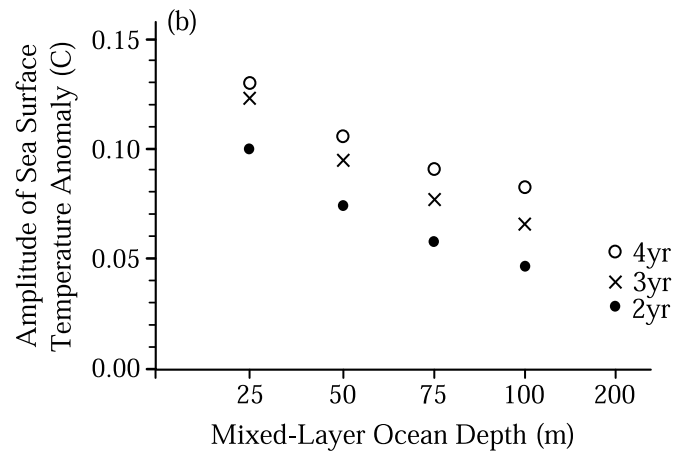
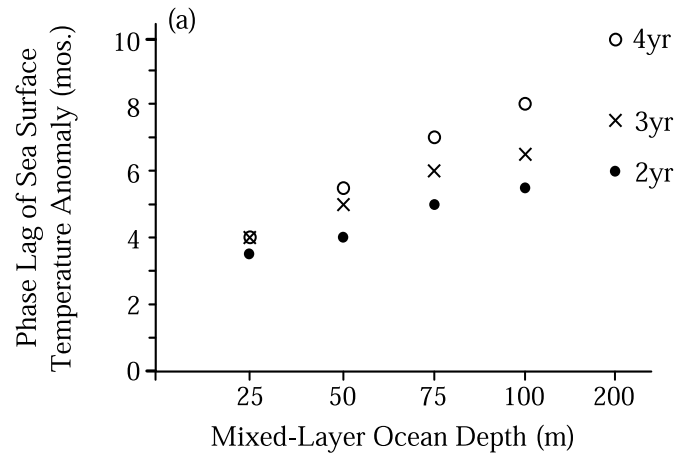


Figure 12

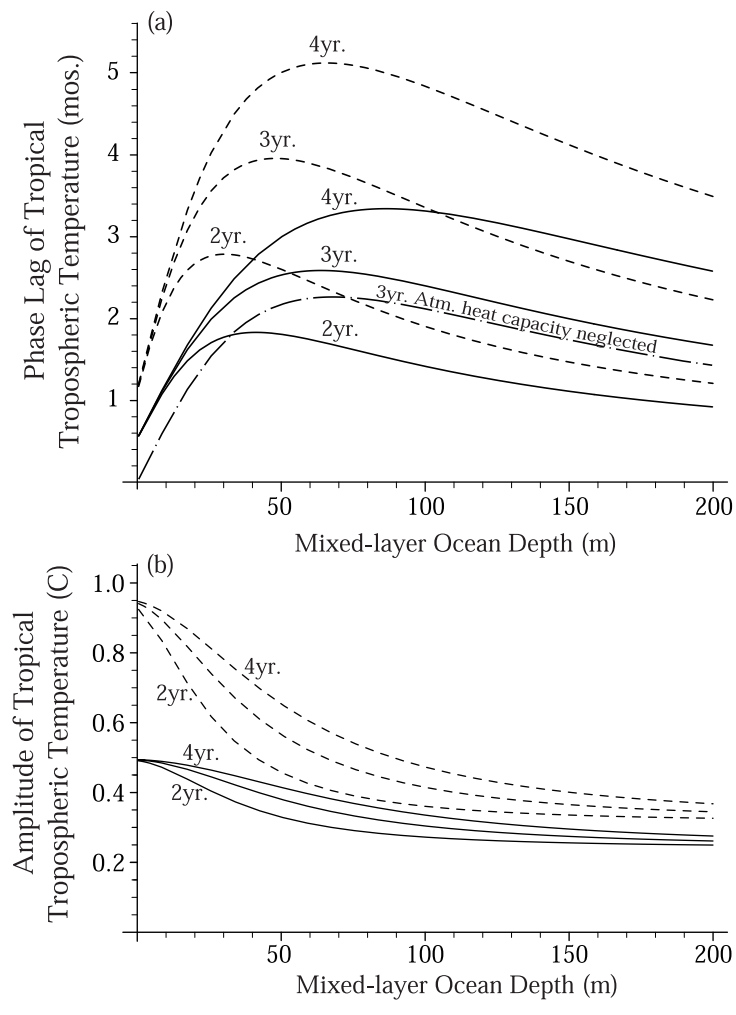


Figure 13

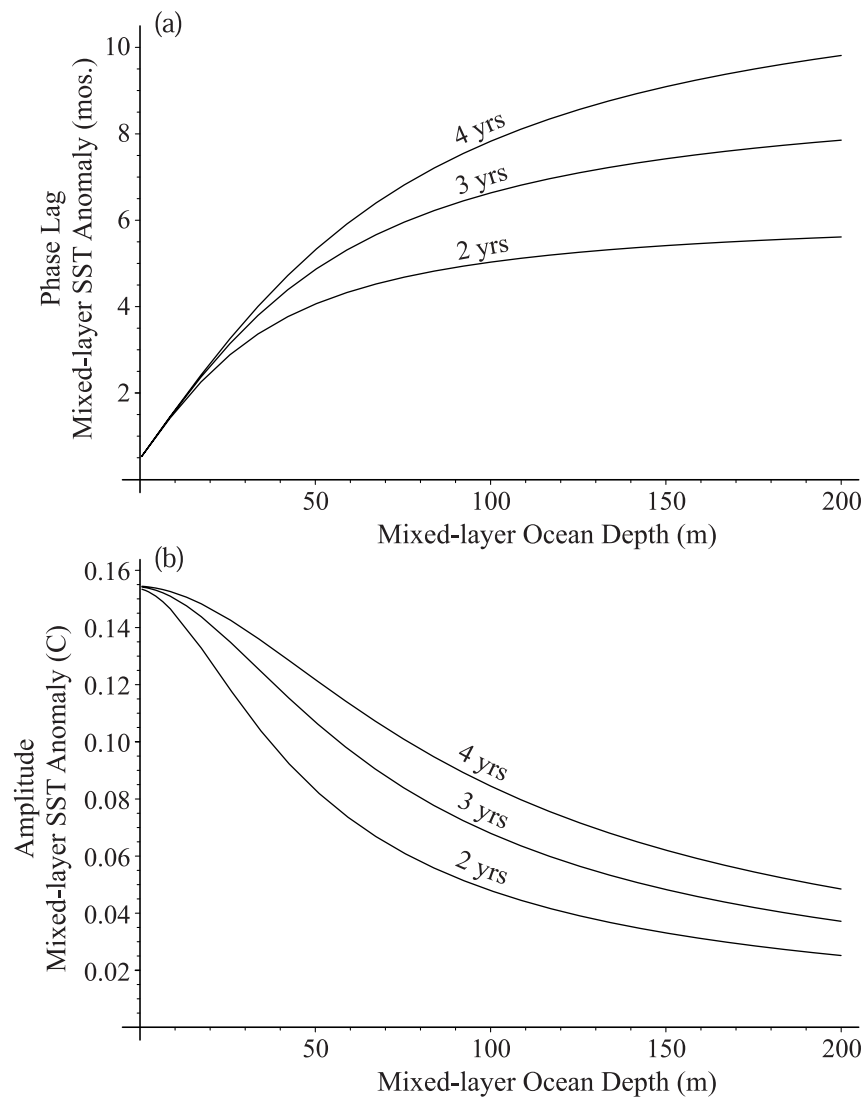


Figure 14

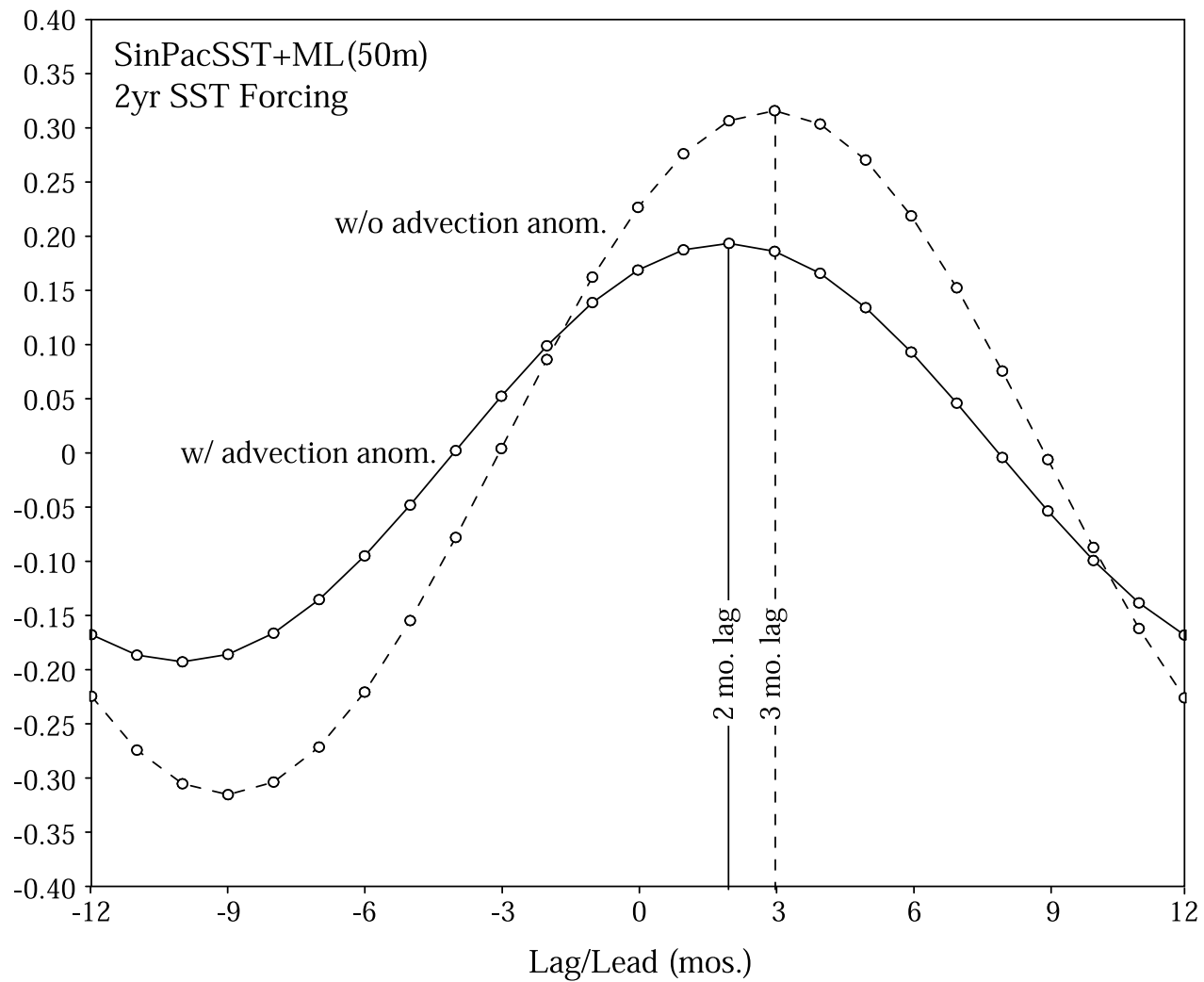


Figure 15

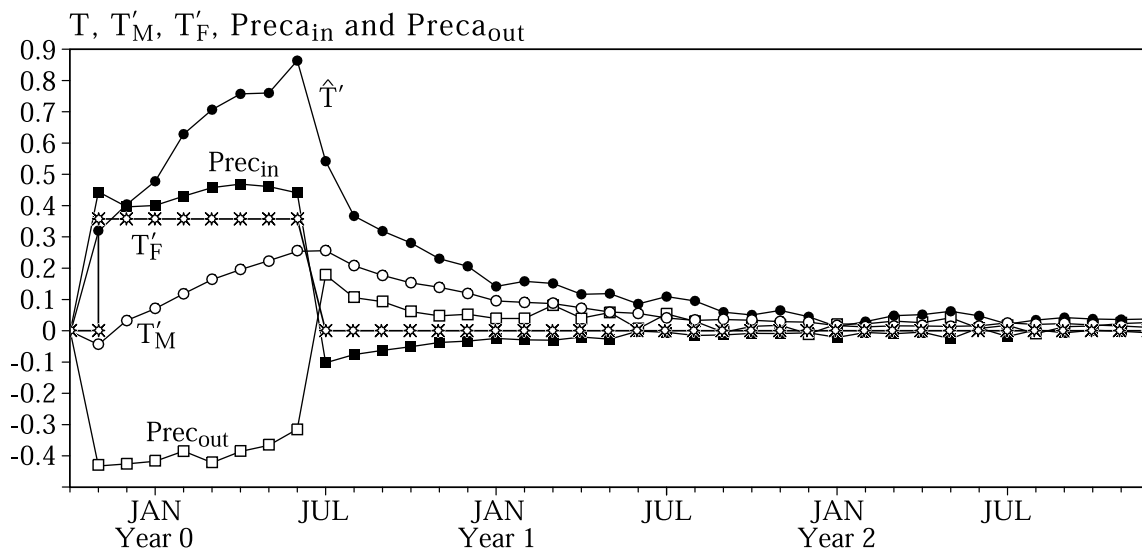


Figure 16